BBA - General Subjects 1864 (2020) 129609

Contents lists available at ScienceDirect

BBA - General Subjects

journal homepage: www.elsevier.com/locate/bbagen

Human importin α3 and its N-terminal truncated form, without the importin-β-binding domain, are oligomeric species with a low conformational stability in solution

Clara Díaz-García[a,1], Felipe Hornos[b,1], A. Marcela Giudici[b], Ana Cámara-Artigas[c], Juan Román Luque-Ortega[d], Arantxa Arbe[e], Bruno Rizzuti[f], Carlos Alfonso[d], Jade K. Forwood[g], Juan L. Iovanna[h], Javier Gómez[b], Manuel Prieto[a], Ana Coutinho[a,i], José L. Neira[b,j,*,1]

[a] iBB- Institute for Bioengineering and Bioscience, Instituto Superior Técnico, Universidade de Lisboa, 1049-001, Lisboa, Portugal
[b] IDIBE, Universidad Miguel Hernández, 03202 Elche, Alicante, Spain
[c] Departamento de Química y Física, Research Center CIAIMBITAL, Universidad de Almería- ceiA3, 04120 Almería, Spain
[d] Centro de Investigaciones Biológicas Margarita Salas (CSIC), Ramiro de Maeztu 9, 28040 Madrid, Spain
[e] Centro de Física de Materiales (CFM) (CSIC-UPV/EHU), Materials Physics Center (MPC), 20018 San Sebastián, Spain
[f] CNR-NANOTEC, Licryl-UOS Cosenza and CEMIF.Cal, Department of Physics, University of Calabria, Via P. Bucci, Cubo 31 C, 87036 Arcavacata di Rende, Cosenza, Italy
[g] School of Biomedical Sciences, Charles Sturt University, Wagga Wagga, NSW 2678, Australia
[h] Centre de Recherche en Cancérologie de Marseille (CRCM), INSERM U1068, CNRS UMR 7258, Aix-Marseille Université and Institut Paoli-Calmettes, Parc Scientifique et Technologique de Luminy, 163 Avenue de Luminy, 13288 Marseille, France
[i] Departamento de Química e Bioquímica, Faculdade de Ciências, Universidade de Lisboa, 1649-004 Lisboa, Portugal
[j] Instituto de Biocomputación y Física de Sistemas Complejos, Joint Units IQFR-CSIC-BIFI, and GBsC-CSIC-BIFI, Universidad de Zaragoza, 50009 Zaragoza, Spain

ARTICLE INFO

Keywords:
Circular dichroism
Fluorescence
Importins
Protein-stability
Self-association

ABSTRACT

Background: Eukaryotic cells have a continuous transit of macromolecules between the cytoplasm and the nucleus. Several carrier proteins are involved in this transport. One of them is importin α, which must form a complex with importin β to accomplish its function, by domain-swapping its 60-residue-long N terminus. There are several human isoforms of importin α; among them, importin α3 has a particularly high flexibility.
Methods: We studied the conformational stability of intact importin α3 (Impα3) and its truncated form, where the 64-residue-long, N-terminal importin-β-binding domain (IBB) has been removed (ΔImpα3), in a wide pH range, with several spectroscopic, biophysical, biochemical methods and with molecular dynamics (MD).
Results: Both species acquired native-like structure between pH 7 and 10.0, where Impα3 was a dimer (with an apparent self-association constant of ~10 μM) and ΔImpα3 had a higher tendency to self-associate than the intact species. The acquisition of secondary, tertiary and quaternary structure, and the burial of hydrophobic patches, occurred concomitantly. Both proteins unfolded irreversibly at physiological pH, by using either temperature or chemical denaturants, through several partially folded intermediates. The MD simulations support the presence of these intermediates.
Conclusions: The thermal stability of Impα3 at physiological pH was very low, but was higher than that of ΔImpα3. Both proteins were stable in a narrow pH range, and they unfolded at physiological pH populating several intermediate species.
General significance: The low conformational stability explains the flexibility of Impα3, which is needed to carry out its recognition of complex cargo sequences.

Abbreviations: AB, antibody; AFM, atomic force microscopy; ANS, 1-anilino-8-naphtalene sulfonate; ARM, armadillo; AUC, analytical ultracentrifugation; BN-PAGE, blue native poly-acrylamide gel electrophoresis; CD, circular dichroism; DLS, dynamic light scattering; DSC, differential scanning calorimetry; GdmCl, guanidinium hydrochloride; IBB, importin-β-binding; Impα3, human importin α3 isoform (residues 1–521); ΔImpα3, truncated species of Impα3 (residues 64–521), depleted of the IBB domain; IRF, instrument response function; ITC, isothermal titration calorimetry; MD, molecular dynamics; MW, molecular weight; NLS, nuclear localization sequence; NPC, nuclear pore complex; PVDF, Polyvinylidene fluoride; SV, sedimentation velocity; UV, ultraviolet; VIS, visible; WB, western-blot.

* Corresponding author at: IDIBE, Edificio Torregaitán, Universidad Miguel Hernández, Avda. del Ferrocarril s/n, 03202 Elche, Alicante, Spain.
E-mail address: jlneira@umh.es (J.L. Neira).
[1] These authors contributed equally to this work.

https://doi.org/10.1016/j.bbagen.2020.129609
Received 1 November 2019; Received in revised form 13 March 2020; Accepted 26 March 2020
Available online 29 March 2020

1. Introduction

The active transport of proteins from the cytoplasm to the nucleus occurs through a family of transport receptors known as importins (or karyopherin) together with other proteins as the GTPase Ran and nucleoporins [1,2]. Although importin β can recruit some proteins (cargos) directly [3], the classical nuclear import pathway is initiated by recognition of a typical nuclear localization sequence (NLS) in the cargo by importin α [4]. The complex cargo-importin α binds to importin β; this ternary complex moves through the nuclear pore complex (NPC) by using interactions with the phenylalanine–glycine repeats present in nucleoporins [5]. Once the ternary complex is within the nucleus, the GTPase Ran dissociates it by interacting with importin β, and both the importins α and β are recycled back to the cytoplasm [4]. Directionality of the transport is provided by a Ran-GTP gradient, which is guaranteed mainly by the GTP-bound species within the nucleus and by the GDP-bound species in the cytoplasm [6]. However, importin α can accumulate in the nucleus due to cellular stresses, resulting in a blockade of the classical nuclear import pathway [4,7,8] and leading in some cases to the development of a few cancer types [9]. The human genome encodes seven isoforms of importin α, divided into three subtypes [4,10,11]. These isoforms play key roles in cancer development, cell differentiation, gene regulation [10,12], and even in viral infections, as some viral proteins are recognized by specific importins ([13] and references therein).

Both importins α and β are modular proteins built of α-helix repeat units [1,4]. Importin β is formed by 19 tandem HEAT repeat units, each made of two α-helices, folded in a super-helical fashion [14,15]. On the other hand, importin α includes: (i) an N-terminal importin β-binding (IBB) domain, roughly 60-residue-long, which is used for binding to importin β before transport through the NPC; and (ii) a C-terminal NLS binding motif formed by ten armadillo (ARM) repeat units [16]. Each ARM unit is formed by three α-helices [4], and the ten units in importin α adopt a super-helical twist generating an elongated molecule. Several structures of truncated importin α, without the IBB domain ([13] and references therein), have shown that the cargo NLS region binds in an extended and anti-parallel conformation in a concave site of the elongated structure involving ARM motifs 2–4 (major site) or 6–8 (minor site) for the shortest classical monopartite NLSs, or both sets of ARM motifs for the largest bipartite NLSs. In the absence of importin β, the IBB domain, which mimics an NLS region, occupies the ARM motifs involved in NLS recognition [16]. This intramolecular interaction has an auto-inhibitory role, and it is thought to be relevant in cargo dissociation in the nucleoplasmic side [16]. Whereas this intramolecular auto-inhibition seems to be common to all importins, some isoforms have developed other ways of auto-regulation; for instance, the solved crystal structure of a truncated species of importin α1, without the IBB domain, has shown an auto-inhibition mode involving self-association [17]. Furthermore, the flexibility among the different isoforms is also different, and for example, it has been suggested that importin α3 (Impα3) has a higher flexibility than other isoforms, which allows to bind partners containing topologically complex NLS sequences [13,18–20].

In this work, we have studied the conformational stability of Impα3, and that of its truncated species, without the IBB domain (ΔImpα3), in aqueous solution by using several spectroscopic and biophysical techniques, namely, steady-state and time-resolved fluorescence intensity and anisotropy measurements, circular dichroism (CD), dynamic light scattering (DLS), analytical ultracentrifugation (AUC), small angle X-ray scattering (SAXS), western-blots (WB), differential scanning calorimetry (DSC), blue native poly-acrylamide gel electrophoresis PAGE (BN-PAGE) and molecular dynamics (MD) simulations. Our results indicate that both proteins were oligomeric at physiological pH, and they acquired a native-like topology above pH 7.0 (whereas below that pH both proteins precipitated). The stability of both proteins at pH 7.8 was small, with apparent denaturation midpoints around 331 K (58 ºC) for Impα3 and 323 K (50 ºC) for ΔImpα3, as determined by DSC, although both heat-denaturation processes were strongly irreversible, showing a scan-rate-dependent temperature of denaturation. Thermal denaturations at physiological pH, followed by using CD and fluorescence, led to the observation of different midpoint values, indicating the presence of thermal intermediates. For ΔImpα3, MD simulations gave indications on the structure of such intermediate. Furthermore, experiments indicated that GdmCl-chemical denaturations were also irreversible, and showed the presence of intermediate species during unfolding, with non-native structure of the oligomers, and then their dissociation and concomitant unfolding of the monomer.

2. Materials and methods

2.1. Materials

Ampicillin and isopropyl-β-D-1-tiogalactopyranoside were obtained from Apollo Scientific (Stockport, UK). Imidazole, kanamycin, Trizma base and His-Select HF nickel resin were from Sigma-Aldrich (Madrid, Spain). Triton X-100, Tris(2-carboxyethyl)phosphine (TCEP) and protein marker (PAGEmark Tricolor) were from VWR (Barcelona, Spain). Amicon centrifugal devices with a cut-off molecular weight of 30 or 50 kDa were from Millipore (Barcelona, Spain). The rest of the used materials were of analytical grade. Water was deionized and purified on a Millipore system.

2.2. Protein expression and purification

Expression and purification of codon-optimized, His-tagged ΔImpα3 (residues 64–521) were carried out in BL21 (DE3) cells as described [13]. The DNA of the codon-optimized, intact Impα3 was synthesized by NZytech (Lisbon, Portugal) and cloned into the pHTP1 vector (with kanamycin resistance), and with a His-tag at the N terminus. Expression and purification of Impα3 were carried out as those of ΔImpα3 in the same *E. coli* strain cells. Protein concentration of both species was determined from the absorbance at 280 nm of their six tyrosines and six tryptophans [21].

2.3. Fluorescence

2.3.1. Steady-state fluorescence

Fluorescence spectra were collected on a Cary Varian spectrofluorometer (Agilent, Santa Clara, CA, USA), interfaced with a Peltier unit. All experiments were carried out at 298 K (25 °C). Following the standard protocols used in our laboratories, the samples were prepared the day before and left overnight at 278 K (5 °C); before experiments, samples were left for 1 h at 298 K (25 °C). A 1-cm-pathlength quartz cell (Hellma, Belgium) was used.

For the pH-denaturation experiments, protein samples were excited at 280 and 295 nm in the pH range from 2.0 to 12.0. The other experimental parameters and the buffers used have been described elsewhere [22,23]. Appropriate blank corrections were made in all spectra. Protein concentration was 4 μM for both species (in protomer units). The pH of each sample was measured after completion of pH-denaturations with an ultra-thin Aldrich electrode in a Radiometer (Copenhagen, Denmark) pH-meter.

Chemical-denaturations at pH 7.8 (phosphate buffer), either followed by fluorescence or CD, were carried out by dilution of the proper amount of a 7 M GdmCl stock solution. The concentration in the stock GdmCl solution was quantified using refractive index measurements [24]. All the denaturations were irreversible (Section 3) for both species at a concentration of 4 μM (in protomer units) (Fig. SM 1), especially at the low denaturant concentrations (Section 3.4).

2.3.2. Thermal-denaturations

The thermal-denaturations were performed at constant heating rates

of 60 K/h with an average time of 1 s. Thermal scans were collected at 315, 330 and 350 nm after excitation at either 280 or 295 nm, from 298 (25 °C) to 358 K (85 °C). The rest of the experimental set-up was the same described above. The thermal denaturations for both species were irreversible (Section 3.1). Irreversibility was tested by acquiring steady-state spectra after thermal denaturation, and by comparing their shape and intensity with those of the spectra acquired before heating. The apparent thermal denaturation midpoint was estimated from a two-state equilibrium equation as described [23].

2.3.3. 1-anilino-8-naphtalene sulfonate (ANS) binding

The excitation wavelength was 380 nm, and emission was measured from 400 to 600 nm at 298 K (25 °C). Slit widths were 5 nm for both excitation and emission. ANS stock solutions were prepared in water and diluted to yield a final concentration of 100 μM, with final protein concentrations of 4 μM for both importins (in protomer units). Spectra from blank solutions were subtracted from the corresponding spectra containing either protein. ANS was used to monitor the pH-denaturations of both species and their GdmCl-denaturation at pH 7.8. The pH of each sample was measured after completion of pH-denaturations with an ultra-thin Aldrich electrode in a Radiometer pH-meter.

2.3.4. Steady-state and time-resolved fluorescence intensity and anisotropy measurements

The steady-state fluorescence anisotropies of Impα3 and ΔImpα3 were measured at 298 K (25 °C) on a Horiba Jobin Yvon Fluorolog-3-21 spectrofluorometer (Kyoto, Japan) by using 0.5 cm × 0.5 cm quartz cuvettes (Hellma, Belgium), according to:

$$\langle r \rangle_{ss} = \frac{I_{VV} - GI_{VH}}{I_{VV} + 2GI_{VH}} \quad (1)$$

where I_{VV} and I_{VH} are the fluorescence intensities (after subtraction of the blank) of the vertically and horizontally polarized emission respectively, both recorded when the sample is excited with vertically polarized light. The instrumental *G*-factor ($G = I_{VH}/I_{HH}$) corrects the measurements for the bias in detecting the vertically and horizontally polarized components of the emission. The excitation and emission wavelengths were 300 nm and 345 nm, respectively, with 5 nm slit widths in both cases.

The fluorescence intensity decays, with picosecond resolution, were obtained for both importins at 298 K (25 °C) by using the time-correlated single-photon timing technique, as previously described [25,26]. Upon excitation at 300 nm, the fluorescence decays, $I(t)$, were measured at 345 nm with an emission polarizer set at the magic angle (54.7°) relative to the vertically polarized excitation beam, produced by a frequency doubled (BBO crystal) Rhodamine 6G laser. The instrument response function (IRF) was recorded as the excitation light scattered by a Ludox solution (silica and colloidal water solution (Aldrich, Milwaukee, USA)). The data were collected using a multichannel analyzer with a time window of 1024 channels, typically using a time scale of 19.5 or 29.3 ps/channel. For measuring the time-resolved fluorescence anisotropy decays, the parallel and perpendicular polarized components of the fluorescence to the vertical plane of polarization of the excitation beam ($I_{VV}(t)$ and $I_{VH}(t)$, respectively) were alternately recorded as previously described [25,26]. The instrumental *G*-factor was calculated using the steady-state anisotropy of the sample as a constraint [27]. As expected, the *G*-factor values were always found to be close to 1 ($0.9 < G < 1.1$).

The fluorescence intensity and anisotropy decays were analyzed using the 1.4 version of the TRFA software (Scientific Software Technologies Center, Minsk, Belarus). The statistical criteria, namely a reduced χ^2 value < 1.3 and a random distribution of the residuals and autocorrelation plots around zero, were used to evaluate the goodness of the fits. The TRFA software allows for the automatic calculation of the confidence intervals corresponding to one standard deviation for each fitted parameter [27].

The fluorescence intensity decay curves, $I(t)$, were described by a sum of discrete exponential terms ($n = 3$):

$$I(t) = \sum_{i=1}^{n} \alpha_i \exp(-t/\tau_i) \quad (2)$$

where α_i and τ_i are, respectively, the amplitude and lifetime of the *i*th decay component. The intensity-weighted mean fluorescence lifetime, $< \tau >$, was calculated according to:

$$\langle \tau \rangle = \frac{\sum_{i=1}^{n} \alpha_i \cdot \tau_i^2}{\sum_{i=1}^{n} \alpha_i \cdot \tau_i} \quad (3)$$

The time-resolved anisotropy decays, $r(t)$, were globally analyzed and described according to:

$$r(t) = \sum_{i=1}^{n} \beta_i \exp(-t/\phi_i) \quad (4)$$

where β_i and ϕ_i are the normalized amplitude and the rotational correlation time of the *i*th decay component, respectively.

The self-association studies of both importins at pH 8.0 were carried out in a range of protein concentrations from 2.5 to 20 μM (in protomer units). In the equilibrium unfolding studies, the protein concentration was kept fixed at 7.5 μM (of protomer concentration for both proteins) and the GdmCl concentration was varied from 0 to 6 M in 50 mM Tris-HCl, pH 8.0 buffer. We had to use such a larger concentration (when compared to that used in equilibrium techniques, 4 μM) because a longer excitation wavelength (300 nm) was used in these experiments.

2.4. CD

Far-UV CD spectra were collected on a Jasco J810 spectropolarimeter (Jasco, Japan) with a thermostated cell holder, and interfaced with a Peltier unit at 298 K (25 °C). The instrument was periodically calibrated with (+)-10-camphorsulphonic acid. A path length cell of 0.1 cm was used (Hellma, Belgium). All spectra were corrected by subtracting the corresponding baseline. Concentration of each protein species was 4 μM (in protomer units). Molar ellipticity was calculated as described [23].

2.4.1. Far-UV spectra

Isothermal wavelength spectra of both proteins at different pH values or GdmCl concentrations were acquired at a scan speed of 50 nm/min with a response time of 2 s, a band-width of 1 nm, and averaged over six scans. Both, the chemical- and pH-denaturations were repeated at least three times with new samples. The samples were prepared the day before and left overnight at 278 K (5 °C) to allow for equilibration. Before starting the experiments, samples were left for 1 h at 298 K (25 °C).

2.4.2. Thermal-denaturations

The experiments were performed at constant heating rates of 60 K/h and a response time of 8 s. Thermal scans were collected by following the changes in ellipticity at 222 nm from 298 (25 °C) to 353 K (80 °C). The rest of the experimental set-up was the same reported in the steady-state experiments. No difference was observed between the scans aimed to test drifting in the signal of the spectropolarimeter. Thermal-denaturations were not reversible at any pH for any of the two proteins, as shown by: (i) the comparison of spectra before and after the heating; and, (ii) the changes in the voltage of the instrument detector [28]. The apparent thermal- denaturation midpoint was estimated from a two-state equilibrium equation as described [23].

2.5. Dynamic Light Scattering (DLS)

DLS measurements were performed in a Zetasizer Nano instrument (Malvern Instruments Ltd., UK) equipped with a 10 mW helium-neon laser (λ = 632.8 nm) and a thermoelectric temperature controller. All the experiments were performed at a fixed angle (Θ = 173°) at 298 K (25 °C) and were analyzed with Zetasizer software V7.12 (Malvern Instruments Ltd., UK). Before each measurement, samples of Impα3 and ΔImpα3 were centrifuged for 30 min at 14,000 *g* and filtered in a 0.2 μm cut-off Millex filter to remove large aggregates and dust. Once in the cuvette, samples were sonicated 1 min to remove bubbles. Each sample was measured 10 times with 10 runs of 30 s each. The *Z*-average size was obtained by fitting the autocorrelation function with the cumulants method. The hydrodynamic radius, R_h, of the molecule was calculated by applying the Stokes-Einstein equation:

$$D = kT/(6\pi\eta R_h) \quad (5)$$

where D is the translational diffusion coefficient, k is the Boltzmann constant, T is the temperature and η is the solution viscosity.

2.6. BN-PAGE

BN-PAGE was performed in linear 4–16% (*w/v*) polyacrylamide-gradient gels [29–31]. Before starting, sample aliquots (15 μL) of 39 μM Impα3 and 26 μM ΔImpα3 proteins were mixed with 1 μL 5% (w/v) Coomassie Brilliant blue G stock solution in 750 mM aminocaproic acid. Electrophoresis was initiated at 85 V for 30 min, then continued at 200 V for 2.5 h, at 277 K (4 °C). After electrophoresis, the gels were stained overnight with colloidal Coomassie Blue G 250.

2.7. Western-blot (WB)

Electrophoresis was carried out as explained above. The selected SDS concentration to see Impalpha3 and ΔImpalpha3 was 20 mM. Proteins were then electroblotted from the gel onto a (Polyvinylidene fluoride) PVDF membrane at 30 V overnight. Blots were treated with 62.5 mM Tris–HCl (pH 6.8), 2% SDS for 1 h at 50 °C, dried and activated in methanol for 30 s to eliminate the Coomassie blue dye, which interferes in immunodetection. After washing in TBST buffer (50 mM Tris–HCl pH 7.4, 25 mM NaCl, 0.05% Tween 20), blots were processed for WB by blocking in 3% (*w/v*) bovine serum albumin in TBST, then incubated with a rabbit polyclonal anti-KPNA4 antibody (AB) (1:2000, Quimigen) and diluted in the blocking solution. After washing, the immunoblots were incubated with a secondary AP-conjugated goat anti-rabbit IgG (1:3000, Proteintech). Immunoreactive proteins were visualized by nitroblue tetrazolium (NBT)/5-bromo-4-chloro-3-indolyl phosphate (BCIP) precipitation by alkaline phosphatase.

2.8. Analytical ultracentrifugation (AUC) sedimentation velocity (SV) assay

Samples of protein Impα3 and ΔImpα3 at 22 μM, in 50 mM Tris, pH 8, were loaded (400 μL) into 12 mm epon-charcoal standard double-sector centerpieces. The assay was performed at 293 K (20 °C) and 48,000 rpm in an XL-A analytical ultracentrifuge (Beckman-Coulter Inc.) equipped with a UV-VIS absorbance detection system, using an An-50Ti rotor. Sedimentation profiles were recorded by using the absorbance at 280 nm. Differential sedimentation coefficient distributions were calculated by least-squares boundary modelling of sedimentation velocity data using the continuous distribution *c(s)* Lamm equation model as implemented by SEDFIT [32]. These experimental *s* values were corrected to standard conditions using the program SEDNTERP [33] to obtain the corresponding standard *s* values ($s_{20,w}$).

2.9. SAXS

SAXS experiments were conducted on a Rigaku 3-pinhole PSAXS-L equipment operating at 45 kV and 0.88 mA. The MicroMax-002+ X-ray Generator Systems is composed by a microfocus sealed tube source module and an integrated X-ray generator unit which produces Cu-K_α transition photons of wavelength λ = 1.54 Å. The flight path and the sample chamber were under vacuum. The scattered X-rays were detected on a two-dimensional multiwire X-ray detector (Gabriel design, 2D-2000×). The azimuthally averaged scattered intensities were obtained as a function of scattering vector Q ($Q = 4\pi\lambda^{-1}\sin\theta$, where θ is half the scattering angle). Reciprocal space calibration was done using silver behenate as standard. The solutions were filling boron-rich capillaries with an outside diameter of 2 mm and a wall thickness of 0.01 mm. The contribution from the corresponding buffer (measured on the same capillary) was subtracted by applying the proper factors obtained from transmission measurements. The sample-detector distance was 2 m, allowing the coverage of a Q-range from 0.008 to 0.2 $Å^{-1}$. Experiments were carried out at 298 K (25 °C).

From the intensity scattered at low-Q values –in the so-called Guinier regime– we can determine the average gyration radius, R_g, of the protein, by using the Guinier law:

$$I(Q) = A\exp(-R_g^2Q^2/3) \quad (6)$$

The pre-exponential factor, A, is determined by the molecule concentration, the scattering contrast and the mass of the macromolecules dispersed in the solution. On the other hand, we can estimate the compaction grade of the protein through the scaling exponent, υ, which relates to Q as $I(Q) \approx Q^{-1/\upsilon}$, in the high Q-range here explored. The values of υ are 1/3 for a polymeric chain collapsed into a globule; 0.5 for a random-coil polymer (which is the conformation of a linear polymer chain in Θ-conditions); and 0.6 for a swollen chain in a good solvent (self-avoiding-walk conformation). The form factor of a coil chain, with scaling exponent υ, is described in terms of the so-called generalized Gaussian coil function, given by the expression [34]:

$$I(Q) \approx \frac{1}{\upsilon U^{1/2\upsilon}}\gamma\left(\frac{1}{2\upsilon}, U\right) - \frac{1}{\upsilon U^{1/\upsilon}}\gamma\left(\frac{1}{\upsilon}, U\right) \quad (7)$$

where $U = (2\upsilon + 1)(2\upsilon + 2)Q^2{R_g}^2/6$ and $\gamma(a,x) = \int_0^x t^{a-1}\exp(-t)dt$.

From the fits of this function to the experimental data, the value of R_g can also be obtained.

2.10. Isothermal titration calorimetry (ITC)

The ITC experiments were carried out by using a VP-ITC instrument (Microcal, Northampton, USA). Before the calorimetric experiments, both proteins were concentrated and dialysed at 277 K (4 °C) against 50 mM Tris (pH 8.0). Dilution ITC experiments involved sequential injections of small amounts (25 μL) of a stock of concentrated protein (45 μM of Impα3; and 38 and 118 μM of ΔImpα3) into the calorimetric cell (1.4 mL); the cell initially contained isolated buffer.

2.11. Differential scanning calorimetry (DSC)

DSC experiments were performed on a Nano DSC differential scanning microcalorimeter (TA Instruments, Delaware, USA) with capillary tantalum cells with a total volume of 0.3 mL.

Prior to performing the measurements, protein solutions were dialyzed for 24 h at 277 K (4 °C) against a large volume of the dialysis buffer that was changed three times. The buffer used was 20 mM phosphate at pH 7.0, and the samples were degassed with gentle stirring in an evacuated chamber for 15 min at room temperature and then immediately loaded into the calorimetric cell. The reference cell was filled with the final, degassed dialysis buffer. A pressure of 3 atm of dry nitrogen was always kept over the liquids in both cells throughout the scans in order to prevent any degassing during heating. A background

scan collected with only buffer present in both cells was subtracted from each scan. Four different scan rates were used within the range of about 0.25–2 K/min. For all the experiments the protein concentrations were in the range of 0.5–1 mg/mL (8.6–17.2 μM) for Impα3, and 1.13 mg/mL (22.5 μM) for ΔImpα3. The excess molar heat capacity for protein was plotted *versus* temperature after normalization with respect to the corresponding molecular weights (MWs) ($MW_{Impα3}$ = 57,887 g·mol^{-1}, $MW_{ΔImpα3}$ = 50,202 g·mol^{-1}) using the software package supplied by the instrument.

2.12. Molecular dynamics (MD)

All-atom MD simulations were performed with the GROMACS simulation package [35] to study the dynamical behaviour of ΔImpα3 under denaturing conditions. Simulation runs were carried out at 300, 400, 450 and 500 K (27, 127, 177 and 227 °C) using a computational protocol recently described for high-temperature MD [36,37], and compared with the results obtained at room temperature. The structure of the protein was modelled with the AMBER ff99SB-ILDN force field [38], starting from the crystallographic conformation in a cargo-free state deposited as entry 6BVZ in the Protein Data Bank [13]. The TIP3P water model [39] was used to mimic the protein dynamics under full hydration conditions in explicit solvent. Due to the large negative charge of ΔImpα3, 23 Na^+ counterions were necessary to neutralize the system. Other details of the system preparation (size and shape of the box), computational conditions (modelling of electrostatic and van der Waals interactions, and thermostat/barostat application), and simulation protocol (energy minimization, annealing and equilibration) were as previously described [40,41]. Production runs were carried out for 25 ns in the isobaric-isothermal ensemble, saving data every 1 ps.

3. Results

3.1. Impα3 and ΔImpα3 acquired a native structure in a narrow pH range

To measure the conformational stability of both importins, and address the importance of the IBB domain, we must firstly determine in which pH range Impα3 and ΔImpα3 acquired a native structure. To that end, we used several spectroscopic and biophysical probes, namely intrinsic fluorescence, ANS fluorescence and CD. The use of the whole set of techniques gives complementary information on different structural features of the polypeptide chain. We used intrinsic fluorescence to monitor changes in the tertiary structure of the protein, around its 6 tyrosines and 6 tryptophans. We used ANS fluorescence to monitor the accessibility of solvent-exposed hydrophobic patches, and to detect the presence of possible partially folded species [42]. And, finally, we carried out far-UV CD experiments to monitor changes in the secondary structure of the proteins.

3.1.1. Fluorescence

(1) Steady-state fluorescence and thermal denaturations – The fluorescence emission spectra of both protein species showed a maximum around 345 nm at physiological pH (Fig. SM 1A). This result indicates that the fluorescence in both proteins was dominated by the emission of tryptophans, which appeared to be solvent-exposed.

The fluorescence intensity at 330 nm (either by excitation at 280 or 295 nm) of both proteins showed two transitions at acidic pH values (Fig. 1A and B, blue squares): one around 4.0 and another around 6.0; however, both transitions were associated with sample precipitation occurring between pH 3.5 and 6.5 (indicated with a double-arrow line in Fig. 1). This effect is probably due to the fact that the pI values of both proteins (https://web.expasy.org/protparam) are close to 5.0. In addition, the fluorescence intensity of both species showed a third additional transition occurring at basic pH values (> 10.0), whose pK_a could not be determined due to the absence of baseline at high pH values; this transition must be attributed to the titration of tyrosines. Therefore, both species seemed to acquire a native-like conformation between pH 7.0 and 10.0, and below or above those values both proteins were unfolded.

As below pH 7.0 both proteins did not acquire a native-like conformation, thermal denaturations were carried out at pH 7.8 and 12.1 (Fig. SM 1B and C), after excitation at 280 or 295 nm. At pH 7.8, denaturations were irreversible, and ΔImpα3 had an apparent thermal denaturation midpoint of 323.8 ± 0.2 K (50.8 ± 0.2 °C); and Impα3 of 332.82 ± 0.08 K (59.82 ± 0.08 °C). At pH 12.1, no transition was observed for any of the two proteins, further confirming that the

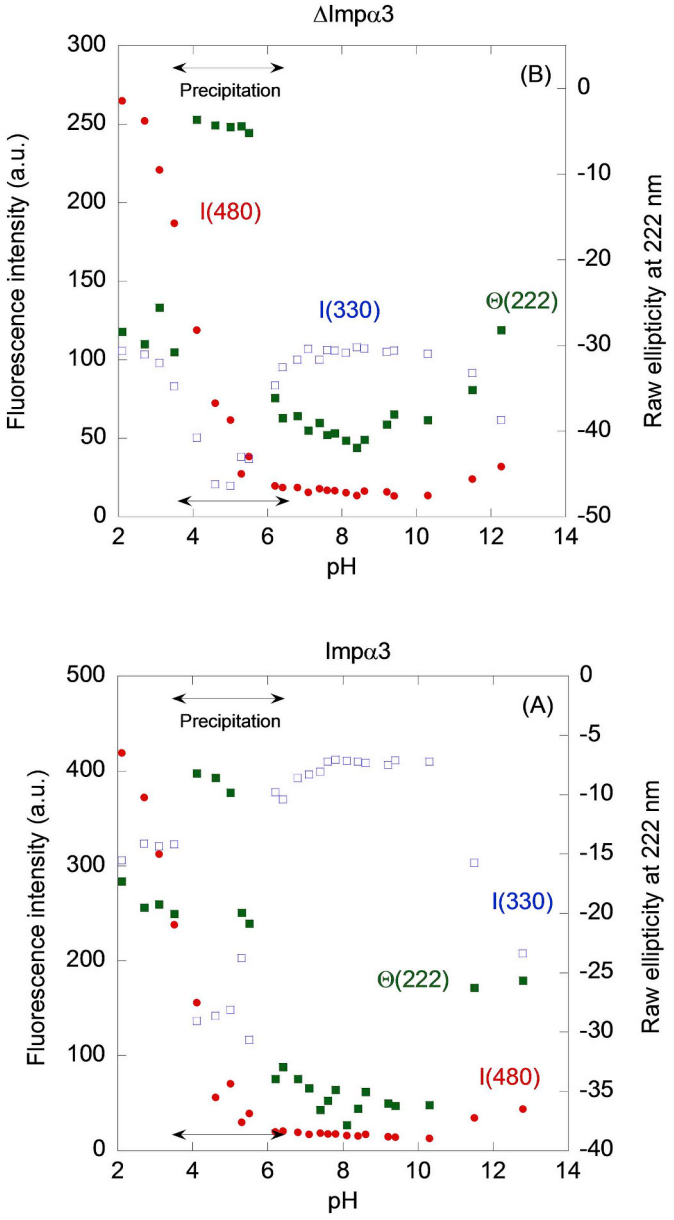

Fig. 1. pH-induced structural changes of Impα3 and ΔImpα3 species followed by spectroscopic techniques. (A) Changes of Impα3 monitored by the intrinsic fluorescence intensity emission at 330 nm, after excitation at 280 nm (blue squares, left axis); scaled-up ANS fluorescence emission at 480 nm (red circles, left axis); and raw ellipticity at 222 nm (green squares, right axis). (B) The same spectroscopic probes as above monitored for ΔImpα3. Experiments were carried out at 4 μM of protein concentration (in both species and for all techniques) and 298 K. The double-arrows at the top and the bottom indicate the pH range where both proteins precipitate in the fluorescence and far-UV CD experiments. (For interpretation of the references to color in this figure legend, the reader is referred to the web version of this article.)

intrinsic fluorescence transition observed at basic pH values must result in the unfolding of both proteins. Moreover, these experiments indicate that the thermal stability of the ΔImpα3 species was lower than that of intact Impα3.

(2) ANS-binding – At low pH, the ANS fluorescence intensity at 480 nm was larger for both species and decreased as the pH was raised (Fig. 1A and B, red squares), suggesting that at low pH, when precipitation was observed, both proteins had solvent-exposed hydrophobic regions. It is interesting to note that we did not observe protein precipitation in the experiments in the presence of ANS, as it has been reported for other proteins [43]. The fluorescence intensity at 480 nm showed a sigmoidal-like behaviour, but we could not determine its pK_a due to the absence of an acidic baseline. At basic pH values (> 10.0), we observed in both proteins an increase in the fluorescence intensity of ANS, which mirrors the decrease in the intrinsic fluorescence signal (Fig. 1, blue squares).

3.1.2. Far-UV CD

The CD spectrum of Impα3 and ΔImpα3 at physiological pH showed minima at 208 and 222 nm (Fig. SM 2A), indicating that both species had mainly helical folds, as it could be expected from the X-ray structures of other isoforms (see for instance [17,20]). Between pH 3.5 and 6.5, we also observed large precipitation in the sample, and from pH 7.0 up to 10.0 ellipticity remained constant, until it decreased (in absolute value) at larger values of pH (Fig. 1A and B, green squares), mirroring the behaviour observed for intrinsic fluorescence (Fig. 1A and B, blue squares) and ANS fluorescence (Fig. 1A and B, red circles) at both extremes of pH, and indicating that at those basic pHs, both species were unfolded. Therefore, the acquisition of secondary structure for both proteins occurred concomitantly to that of the tertiary structure, as monitored by fluorescence and the burial of solvent-exposed hydrophobic residues.

We also carried out thermal denaturations of both proteins at the same pH values used in fluorescence studies (7.8 and 12.1). As it was observed with fluorescence, the thermal denaturations were irreversible at both pH values. At pH 7.8, ΔImpα3 had a thermal denaturation midpoint of 317.9 ± 0.2 K (44.9 ± 0.2 °C); and Impα3 of 325.2 ± 0.4 K (52.2 ± 0.4 °C) (Fig. SM 2B, C). At pH 12.1, we did not observe any sigmoidal transition, further confirming that at basic pHs both proteins were unfolded. We also carried out thermal denaturation experiments followed by CD at pH 3.0 (data not shown) for both proteins, and in either case, we did observe precipitation when samples were heated at relatively low temperatures (~313 K (~40 °C)). These results suggest that: (i) as it happened with fluorescence (see above), the thermal stability of ΔImpα3 was smaller than that of the intact Impα3; (ii) the secondary structure for both proteins, as monitored by

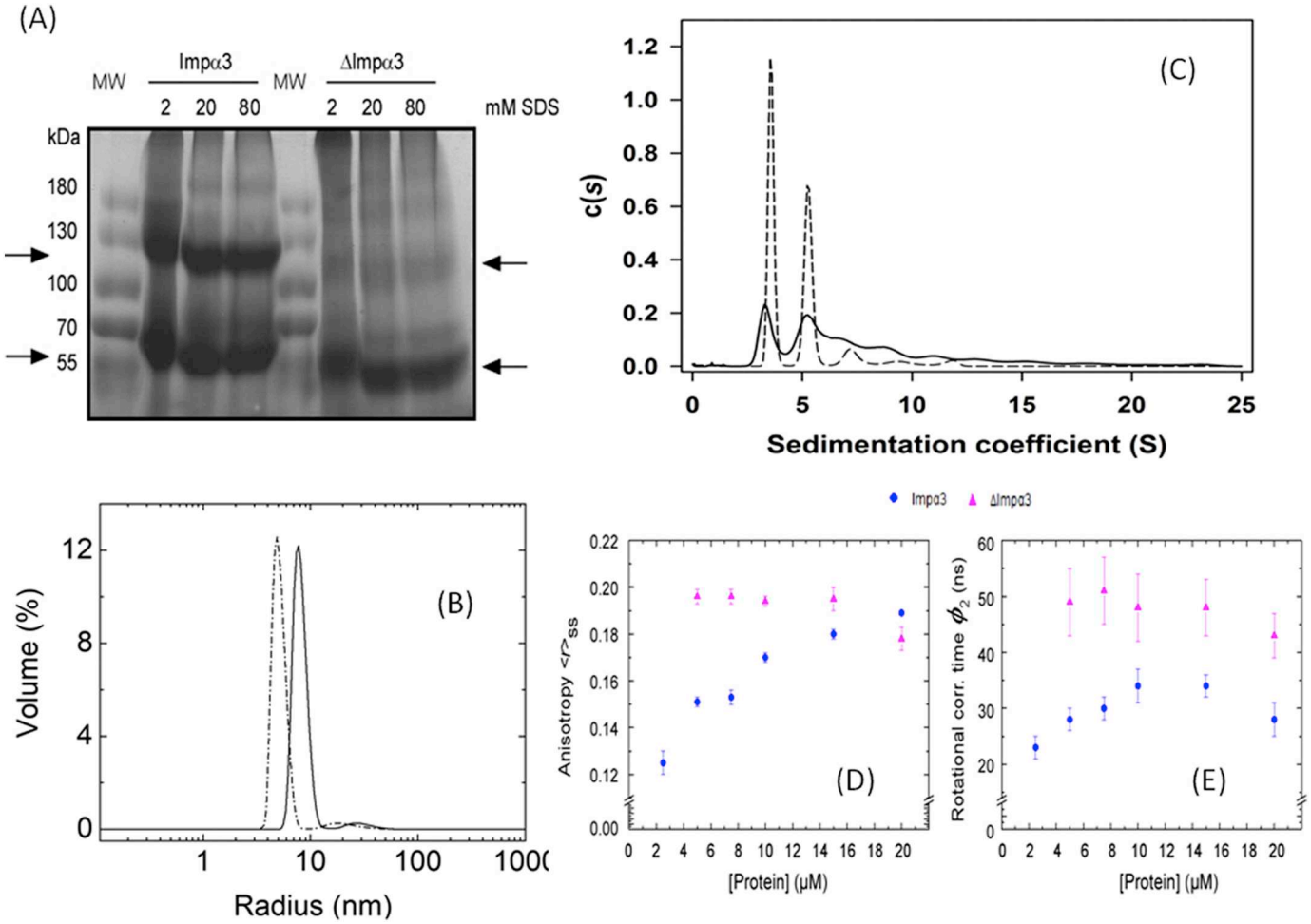

Fig. 2. Self-association states of Impα3 and ΔImpα3: (A) BN-PAGE. Proteins were incubated with different concentrations of SDS before being applied to a BN-PAGE (numbers at the top). Arrows correspond to monomer (the fastest migrating band) and dimer (the slowest migrating band) of Impα3 and ΔImpα3, respectively. MW indicates the molecular weight marker. The numbers at the top indicate the amount of SDS added in the lane (2, 20 and 80 mM). (B) DLS of Impα3 (dot-and-dash line) and ΔImpα3 (continuous line). (C) Sedimentation coefficient distribution profile of Impα3 (dashed line) and ΔImpα3 (continuous line) in solution, obtained by analytical ultracentrifugation SV. (D) Protein-concentration dependence of the steady-state fluorescence anisotropy, $< r >_{ss}$; and of the long rotational correlation time, ϕ_2 (E) for both importins.

CD, seems to melt before the tertiary one, whereas the opposite situation is usually observed with most proteins (this finding is probably due to the large irreversibility of thermal denaturations); and (iii) the transition observed at basic pH (and as discussed above, in correspondence with the titration of the tyrosines) also led to polypeptide chains without any well-fixed secondary structure.

To sum up, for both importins the acquisition of secondary and tertiary structure, as well as the burial of previously solvent-exposed hydrophobic patches, occurred concomitantly. Both proteins acquired a native-like structure within a narrow pH range (7.0 to 10.0) at room temperature.

3.2. Impα3 and ΔImpα3 are oligomeric species in solution at physiological pH

We were interested in elucidating the size and the oligomeric state of both importin species in solution at physiological pH to compare them with those of other importins. To that end, we used several biophysical methodologies which measure different features of a possible self-association process.

First we carried out BN-PAGE and WB experiments, which could be considered choices to study the organization of protein complexes [44–47]. In BN-PAGE, the electrophoretic mobility of the protein is determined by the negative charge from the Coomassie Brilliant Blue, bound to their hydrophobic surface patches. In the presence of 2 mM of SDS (Fig. 2A), both Impα3 and ΔImpα3 exhibited two majority bands capable of entering the gel. The fastest migrating band in the gels was the monomer (indicated by the two bottom arrows), whereas the other gel bands corresponded to dimers (indicated by the two top arrows). It can be seen that the monomer and dimer band of ΔImpα3 had a fastest mobility due to its smaller MW (lowest right arrows) compared to Impα3. The figure also shows that increasing the amount of SDS had no effects on the relative abundances of the supramolecular self-associated species detected by BN-PAGE for each protein. The WB experiments (Fig. SM 3) show that the anti-KPNA4 AB recognizes the monomer of Impα3 and ΔImpα3 (arrow 1), as well as recognizes the dimer of both proteins (arrow 2). Also, the presence of higher-order oligomers can be observed (arrows 3 and 4). Although the bands look very faint in the WB (left side), it should be noted that they are also faint in the BN-PAGE (right side). Then, the two electrophoresis experiments show that both species are oligomeric.

Secondly, DLS was used to determine the R_h of both molecules. Measurements were performed for Impα3 at different concentrations in the range from 5 to 100 μM. Within, the uncertainty of our measurements, the R_h did not change in this concentration range: $R_h = 5.4 \pm 0.4$ nm at 5 μM; $R_h = 5.4 \pm 0.2$ nm at 10 μM; $R_h = 5.3 \pm 0.4$ nm at 20 μM; $R_h = 5.0 \pm 0.1$ nm at 60 μM, and; $R_h = 4.7 \pm 0.3$ nm at 100 μM (Fig. 2B). The average value of R_h (5.2 nm) is higher than that expected for a globular protein of similar MW (for instance, ovoalbumin has MW = 44 kDa, and a $R_h = 2.98$ nm [48]) suggesting that Impα3 had a non-globular fold in solution. Furthermore, the average value of R_h agrees with that determined from the X-ray structures of other importins, which are dimeric (see, for instance, [17]). The Malvern software led to a MW of 138 ± 54 kDa for a $R_h \sim$ 5 nm, for a typical protein similar to a hard sphere.

DLS measurements for ΔImpα3 were performed at three concentrations: 3, 6 and 12 μM. The R_h did not change in this concentration range: $R_h = 8.1 \pm 1.2$ nm at 3 μM; $R_h = 8.1 \pm 0.3$ nm at 6 μM; and $R_h = 8.5 \pm 0.3$ nm at 12 μM (Fig. 2 B). The value of this hydrodynamic radius (average $R_h = 8.3$ nm) suggests that ΔImpα3 was an oligomer in solution in the range of concentrations assayed, and that its shape was larger than that of the intact protein (and therefore, it is more expanded). The Malvern software yielded for ΔImpα3 a MW of 453 ± 147 kDa for a $R_h \sim 8$ nm, for a typical protein similar to a hard sphere.

To determine the possible association state in solution of Impα3 and ΔImpα3, we further subjected both proteins to analytical ultracentrifugation sedimentation velocity (SV) (Fig. 2C). At 22 μM, Impα3 showed two main species, comprising 87% of the sample protein, with experimental sedimentation coefficients of 3.6 S (48.4%) and 5.3 S (38.6%). These values, corrected to standard conditions ($s_{20,w} = 3.7$ S and $s_{20,w} = 5.4$ S, respectively), were compatible with the theoretical values obtained for a slightly elongated Impα3 monomer and dimer (Fig. 2C), respectively. At the same concentration, ΔImpα3 displayed also two peaks at 3.4 S and 5.4 S, that, once corrected to standard conditions ($s_{20,w} = 3.5$ S and $s_{20,w} = 5.5$ S, respectively), were also compatible with the theoretical values obtained for proteins with the corresponding masses for slightly elongated Impα3 monomer and dimer (Fig. 2C). However, ΔImpα3 behaved as a protein with a greater propensity to self-associate, showing not only a higher dimer proportion (29.5%) relative to the monomer (20.9%), but a larger amount of higher-order oligomers (49.6%) than Impα3 (13.0%).

The results of the SAXS experiments with Impα3 led to a $R_g \approx 6$ Å with a $\upsilon \approx 0.43$, close to a compact species value (Fig. SM 4A). Furthermore, the excess of scattering signal at low *Q*-values indicates that the protein was self-associated. On the other hand, the experiments with ΔImpα3 yielded $R_g \approx 7$ Å, with $\upsilon \approx 0.35$, suggesting a larger size for the truncated species than for the intact protein (Fig. SM 4A). Furthermore, there was as well an excess of scattering signal at low Q-values, although it was not as important as in the intact protein.

The influence of protein concentration on the fluorescence properties and rotational dynamics of the full-length and truncated Impα3 were also investigated by using steady-state and time-resolved fluorescence intensity and anisotropy measurements. The fluorescence intensity decays of Impα3 and ΔImpα3 were adequately fitted with a sum of three exponentials (data not shown), presenting a concentration-independent mean fluorescence lifetimes of $< \tau > = 4.9 \pm 0.1$ ns and $< \tau > = 4.4 \pm 0.1$ ns, respectively, within the concentration range explored (2.5–20 μM protomer concentration). This result indicates that the local environment of the tryptophans was slightly different between the full-length and truncated proteins.

The steady-state fluorescence anisotropy, $< r >_{ss}$ of Impα3 was concentration-dependent, progressively decreasing from $< r >_{ss} = 0.189 \pm 0.003$ at 20 μM to $< r >_{ss} = 0.125 \pm 0.003$ at 2.5 μM (Table SM 1). Concomitantly, the fluorescence anisotropy decays, $r(t)$, measured for Impα3, became faster upon protein dilution (Table SM 1). All the measured anisotropy decays for Impα3 (under any conditions) were adequately fitted with two rotational correlation times: a shorter one, ϕ_1, reporting the fast, local dynamics of the tryptophans, which was found to be concentration-independent ($\phi_1 = 0.81 \pm 0.08$ ns); and a longer one, ϕ_2, sensitive to the overall tumbling of the fluorescent species in solution during its excited-state lifetime, which decreased from 38 to 23 ns upon protein dilution (Table SM 1; Fig. 2D and E). Considering the rotation of a spherical protein in solution with an hydration shell of 0.2 g H_2O/g protein and a specific volume of 0.75 mL/g, a theoretical rotational correlation time ϕ_2 of 39.2 ns can be calculated for a dimer of 116 kDa (58 kDa per monomer) [27], which is close to the experimental value measured for Impα3 at 20 μM (Table SM 1). The fact that the rotational properties of Impα3 were affected by its concentration in solution indicates that the protein was involved in a protein-concentration-dependent equilibrium.

At variance with Impα3, both the steady-state and time-resolved fluorescence anisotropy measurements of ΔImpα3 were essentially concentration-independent in the 5–20 μM range explored (Table SM 1), indicating that its self-association constant was higher than that of Impα3. Just like the anisotropy decays of Impα3, those of ΔImpα3 could be adequately fitted with two rotational correlation times (Table SM 1, Fig. 2D and E): ϕ_1 and ϕ_2. A larger value was obtained in this case for the long rotational correlational time $\phi_2 = 48 \pm 3$ ns, suggesting that the oligomerization state of ΔImpα3 was higher than a dimer and/or the shape of the oligomeric species deviated strongly from a spherical geometry, as it was also suggested by the AUC-SV results (Fig. 2C).

This finding must be taken into account when a comparison between the DLS (see above) and anisotropy results is carried out: the MW for ΔImpα3 by using DLS would indicate the presence of octamers. However, such MW was calculated by approximating the protein with a hard sphere, which according to our anisotropy results could not be the case for ΔImpα3.

Finally, we carried out measurements for both species to see whether the proteins dissociated upon dilution, and by measuring the heat uptake in the reaction monitored by ITC. For experiments with Impα3, the heat released upon dilution of the protein into the calorimetric cell was small, and only consistent with a self-dissociation reaction for the first injections, when the concentration in the calorimetric cell was in the low micromolar range (Fig. SM 4B). The amount of heat uptake may reflect the dissociation of the dimeric species; in fact, fitting of a dimer ↔ monomer equilibrium to the experimental data [23] yields a K_d of 17 ± 6 μM, with an enthalpy of 6.9 ± 0.4 kcal/mol (red line in Fig. SM 3B). The value of the K_d, together with the uncertainty in the DLS measurements (see above), can explain why we were not able to determine the presence of such equilibrium by DLS or in the time-resolved fluorescence measurements (even though in the latter we observed some variations). On the other hand, no significant heat evolved upon dilution of ΔImpα3 into the calorimetric cell containing buffer, when protein concentration was 38 μM (Fig. SM 4B) or 118 μM (data not shown). These data suggest that either no self-association was happening (which can be ruled out by the AUC-SV measurements, Fig. 2C, and the SAXS measurements, Fig. SM 4A) or that the dissociation constant is well below the minimum concentration of protein used in the calorimetric cell (the oligomeric form of the protein being the major fraction both in the syringe and in the cell).

Then, to sum up, we can conclude from the array of biophysical and hydrodynamic techniques used that: (i) isolated Impα3 at physiological pH had a tendency to self-associate forming dimers, with a dissociation constant in the low micromolar range; and (ii) isolated ΔImpα3 had a greater tendency than intact Impα3 to self-associate in solution.

3.3. Calorimetric denaturation of Impα3 and ΔImpα3 in solution at physiological pH

3.3.1. A calorimetric point of view

As we have seen by using fluorescence and CD that the thermal stability of ΔImpα3 was smaller than that of intact Impα3 (Figs. SM 1 and SM 2) at physiological pH, but both thermal denaturations were irreversible, we were interested in studying the calorimetric denaturations of both proteins by using differential scanning calorimetry (DSC).

The thermograms of both proteins did not show two transitions, but rather a very broad one. This indicates that, as it happens with thermal denaturations monitored by spectroscopic probes (Figs. S1B and S2B), dissociation and unfolding of the monomers in both proteins occurred concomitantly. The heat-induced denaturation of both proteins was irreversible under all experimental conditions tested, as tested by a second temperature scan of the sample after completion of a first one and cooling. Therefore, the denaturation of both proteins was under

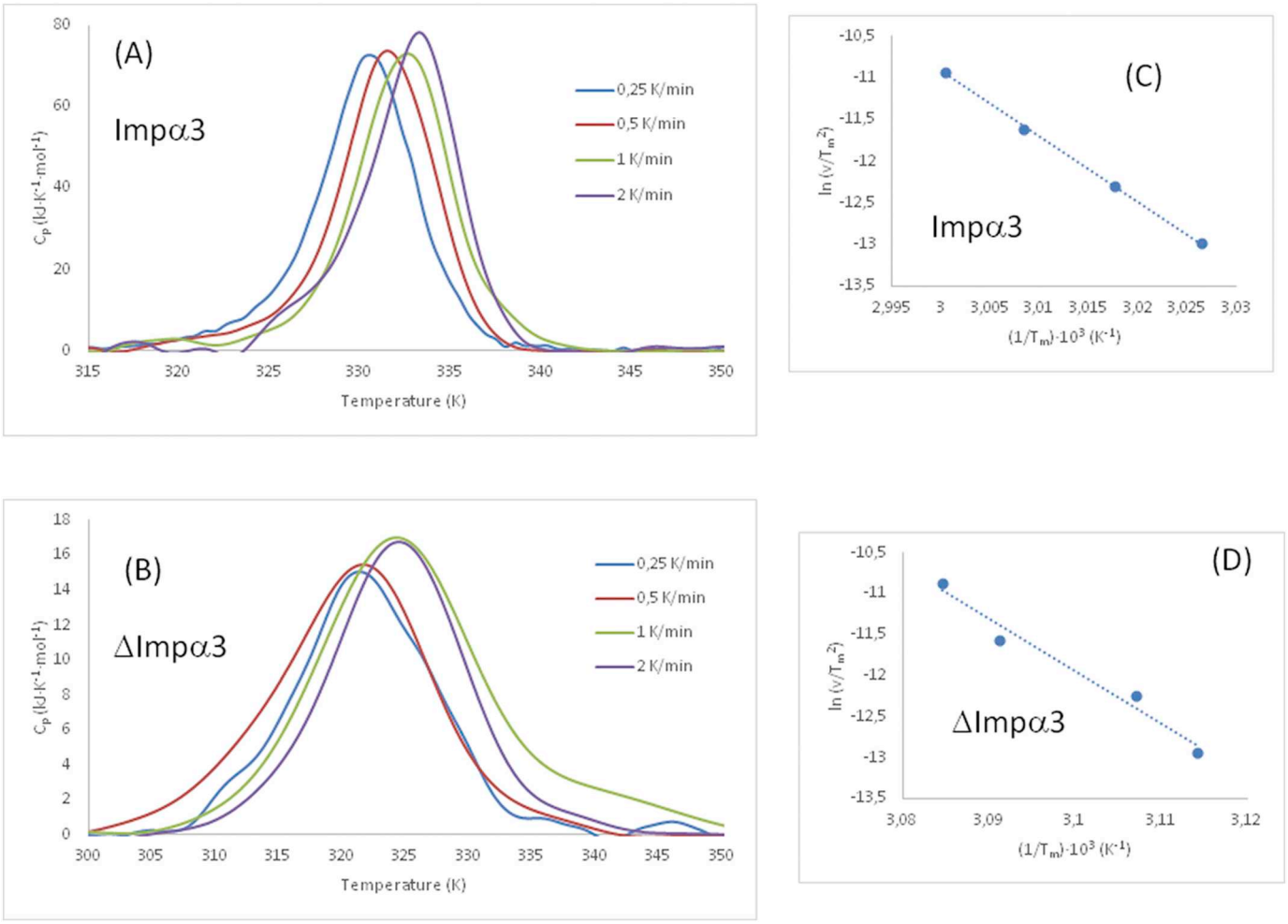

Fig. 3. DSC experiments: Excess molar heat capacity of Impα3 (A) and ΔImpα3 (B) as a function of temperature obtained at four different scan rates: 0.25, 0.5, 1.0 and 2 K/min (°C/min). Plots of ln (ν/T_m^2) *versus* $1/T_m$ for Impα3 (C) and ΔImpα3 (D) according to Eq. (8). Each data point corresponds to one of the four scan rates used in (A) and (B), respectively. The error for each point is estimated to be 10%.

kinetic control and no thermodynamic parameters can be extracted from these experiments. At all scan rates explored, the apparent denaturation midpoints were also lower for ΔImpα3 than for Impα3, confirming previous results obtained by spectroscopic probes (see above); in fact, the apparent denaturation midpoints at 1 K/min (Fig. 3A and B) from the DSC experiments were similar to those obtained by fluorescence (323 (50 °C) and 332 K (59 °C) for ΔImpα3 and Impα3, respectively) (Fig. 3A and B).

The apparent enthalpy change for Impα3, although slightly dependent on the scan rate, has an average value in the order of 500 kJ/mol. Taking into account the size of the protein, this enthalpy value is too low for a complete unfolding, pointing towards the formation of a partially folded state of the protein unable to unfold further upon heating. In fact, we can calculate the expected theoretical value of the enthalpy change by taking into account: (i) the structure of Impα3 (PDB number: 6BVZ); and (ii) the changes in solvent-accessible surface areas of the protein upon unfolding, calculated from its structure, together with the changes in the total buried surface area [49,50]. These calculations led to a theoretical value of the enthalpy of 1220 kJ/mol. This difference between the estimated and the measured enthalpy is even more pronounced for ΔImpα3, as its apparent enthalpy change upon unfolding amounts to only 230 kcal/mol, less than 50% of the value obtained for the intact protein, which is only 15% bigger. Accordingly, our results are consistent with an incomplete unfolding of both proteins and the formation of a partially folded denatured state which might contain a significant amount of both secondary and tertiary structure. In fact, far-UV CD spectra acquired at 348 K (75 °C) had an ellipticity value at 222 nm, which was half of that observed at 293 K (20 °C) for Impα3; and for ΔImpα3, the ellipticity at 222 nm at the higher temperature was more than half the ellipticity at 293 K (20 °C). In addition, the whole far-UV CD spectrum of both proteins was still characteristic of an α-helical protein, suggesting that there is residual helical structure even at those high temperatures.

As expected for a heat-induced denaturation process under kinetic control, the temperature corresponding to the maximum heat capacity, T_m, for both proteins was highly dependent on the scan rate. Considering a two-state irreversible model (that is, assuming that only the native and the final denatured states become significantly populated during the process), the proposed kinetic model predicts that the temperature value corresponding to the maximum of the excess heat capacity curve, T_m, should change with the scan rate according to [51–53]:

$$\ln\left(\frac{\nu}{T_m^2}\right) = A - \frac{E_a}{(RT_m)} \quad (8)$$

where A is a constant; ν is the scan rate; E_a is the activation energy of the kinetically-controlled protein denaturation; and R is the fundamental constant for the ideal gas. Therefore, a plot of ln (ν/T_m^2) *versus* $1/T_m$ should result in a straight line with a slope equal to $-E_a/R$ (Fig. 3C and D). For Impα3, E_a was 650 ± 20 kJ/mol, and for ΔImpα3, it was 530 ± 70 kJ/mol. These values are larger than those measured for other proteins (which are in the range 200–300 kJ/mol), but such difference could be probably due to the fact that the other reported proteins have a smaller polypeptide length [51–53] (the *Bacillus thermoproteolyticus* rokko thermolysin has 340 residues; and carboxypeptidase B and yeast phosphoglycerate kinase both have around 420 amino acids).

3.3.2. A MD simulation point of view

All-atom MD simulations in the presence of explicit solvent were performed to obtain indications on the protein structure during the unfolding process. Because of the size of the protein and of the relatively extended and disordered nature of the IBB domain, *in silico* experiments were carried out only for the ΔImpα3 species, whose crystallographic structure is well characterized [13]. Furthermore, due to necessity to speed up the sampling to have the possibility to observe the unfolding within a time-window accessible to simulations, MD runs were performed at high temperature to decrease the energetic barriers in the denaturation process. Although molecular force fields are not explicitly developed to be employed under extreme temperature conditions, these kind of simulations have proven to be satisfactorily accurate in modelling intermediate states during the unfolding reaction [54,55], and are especially reliable in predicting the early steps of the denaturation process [56], when the protein structure is closer to the folded state rather than being prevalently molten or partially folded.

The Fig. 4A shows the atomic root mean square deviations (RMSDs) from the starting structure obtained after removing (through a least-squares fit on the C^α atoms) the overall roto-translation motion due the protein diffusion, at the different simulation temperatures investigated. At room temperature the RMSD values were 4.1 ± 0.7 Å, consistent with a stable structure of a rather flexible protein. In contrast, at higher temperatures, atomic deviations significantly higher than 5 Å indicated that the unfolding of the protein structure had already started to take place within 5 ns of simulation time. As it could reasonably be expected, the effects observed were larger at the highest sampled temperature, both in terms of the speed of the denaturation process and of the

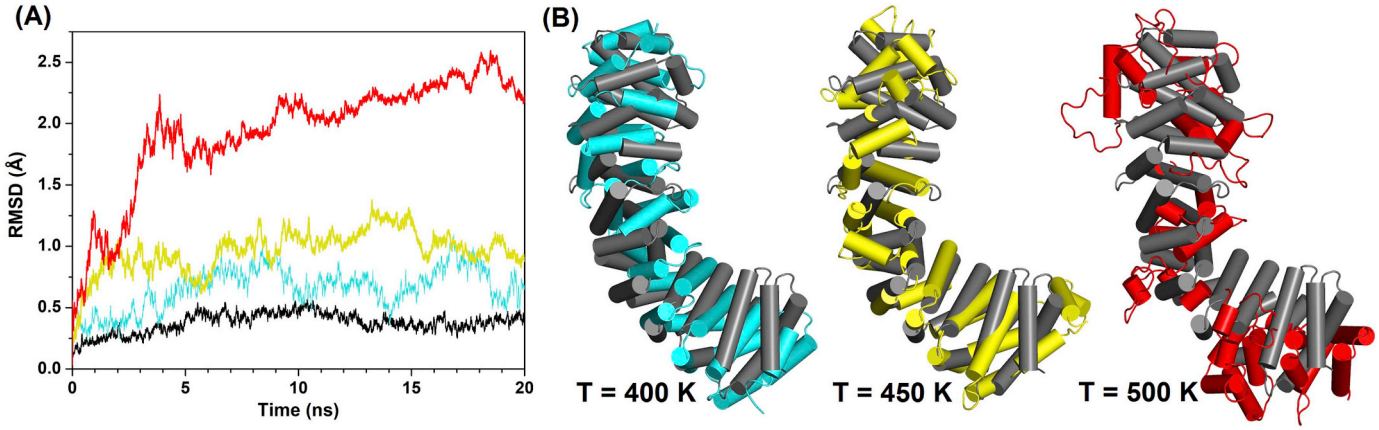

Fig. 4. Simulated model of the early steps of the unfolding of ΔImpα3. (A) Atomic root mean square deviations from the starting structure as a function of simulation time at (black line) 300, (cyan) 400, (yellow) 450, (red) 500 K (27, 127, 177 and 227 °C) (red). (B) Simulated structured at high temperature after 5 ns of simulation; the conformation of ΔImpα3 at room temperature (gray) is superimposed for comparison in each case, by using a least squares fit on the C^α atoms. The protein is shown with helices in cylindrical representation and with the N terminus at the top. (For interpretation of the references to color in this figure legend, the reader is referred to the web version of this article.)

resulting RMSD values from the starting structure.

As summarized by the protein snapshots reported in Fig. 4B, the simulations showed that the unfolding of ΔImpα3 starts with the destabilization and fraying of some helices, triggering a melting of the tertiary structure that ultimately led to a loss of the typical "banana" shape of the protein. This observation agrees with the disruption of the secondary structure before the tertiary structure observed for this protein in our thermal denaturation CD experiments, and is different to the findings commonly reported for most other proteins (see 3.1 and Figs. SM 1 and 2). This apparent experimental discrepancy could be due to the fact the denaturation midpoints were obtained from highly irreversible thermal denaturations (Section 3.1); in addition, it could be possible that the apparent thermal denaturation midpoint report only the presence of a local cluster of residues, as it has been described in other single-tryptophan proteins [57]. Furthermore, our MD results agree with the presence of a large residual amount of both secondary and tertiary structure in the folding intermediate, as we deduced from our calorimetric data (see 3.3.1.) and the CD results at high temperatures. A significant amount of helical structure was also present at the end of the simulated unfolded process (data not shown), although the protein structures obtained later in the denaturation process can be considered less reliable than those observed in the early steps of the process (as discussed above).

It is interesting to note that all our high temperature simulations indicate that ΔImpα3 unfolding progressed through a shift of the ARM repeats units sideways with respect to their longitudinal arrangement along the tertiary structure (Fig. 4B), rather than moving away from each other by determining a further elongation of the super-helical protein arrangement. This finding suggests that the protein does not behave as a sort of highly-loaded molecular spring, at least in the absence of the IBB domain and during the unfolding reaction, at variance with a description of the flexible structure of importin β reported in earlier non-equilibrium MD simulations [58].

3.4. Chemical-denaturation of Impα3 and ΔImpα3 in solution at physiological pH

The irreversible calorimetric measurements indicate that both species dissociate and unfold concomitantly, with the presence of intermediates (as shown by CD, fluorescence and MD simulations), but does the same happen when both proteins were chemically unfolded?

We first tested the reversibility of the chemical denaturations of both proteins using fluorescence and far-UV CD spectroscopies; both techniques allowed us to conclude that the chemical denaturations of Impα3 and ΔImpα3 were not reversible (Fig. SM 5): that is, for both proteins, the denaturation curves of refolded species did not superimpose (neither in the shape nor in the intensity in fluorescence experiments) with the corresponding unfolding curves obtained by using each technique, at least at low GdmCl concentrations. Therefore, we could not obtain any thermodynamic parameter, but we are able to discuss qualitatively the unfolding mechanisms of each protein to obtain clues about the structures of possible intermediates populated along their unfolding pathways.

For Impα3, the different equilibrium spectroscopic techniques (intrinsic fluorescence, ANS-fluorescence and far-UV CD spectra) showed a different behaviour as the denaturant concentration was increased (Fig. 5A), and therefore, we can conclude that the chemical-induced unfolding of this protein was not a two-state process [59]. Whereas intrinsic fluorescence showed a decrease in the intensity at 330 nm until a concentration of ~1.5 M GdmCl was reached, the ANS fluorescence showed a dumb-bell behaviour with a maximum in intensity at ~1.5 M GdmCl. This maximum in the fluorescence intensity of the ANS probe coincides with the onset of the second transition, where the intrinsic fluorescence intensity of the protein followed a quite flat sigmoidal-like curve (from 1.5 to 5 M GdmCl). Therefore, an intermediate species with hydrophobic patches exposed at its surface must be populated at this low denaturant concentration. On the other hand, the far-UV CD results did not show any transition at all in the GdmCl concentration range explored; however although the ellipticity at 222 nm seemed to decrease (in absolute value) in a linear fashion, we cannot rule out the presence of an additional transition at low GdmCl concentrations due to the noise in the observed signal.

To obtain complementary information on the changes in the oligomeric state of the protein, both steady-state and time-resolved fluorescence lifetime and anisotropy measurements were also performed on Impα3 as a function of the GdmCl concentration in solution. Both the fluorescence intensity decays of Impα3 and ΔImpα3 were adequately fitted with a sum of three exponentials (data not shown).

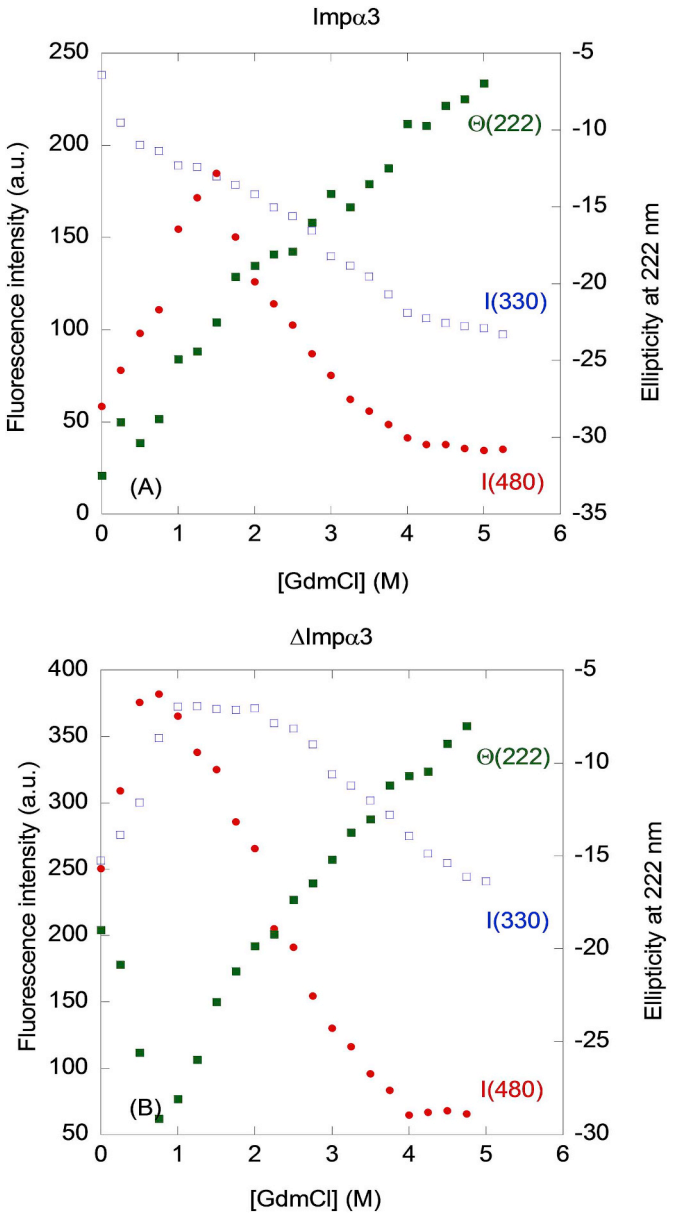

Fig. 5. Chemical denaturations followed by equilibrium techniques. (A) Changes of Impα3 monitored by the intrinsic fluorescence intensity emission at 330 nm, after excitation at 280 nm, (blue squares, left axis); scaled-up ANS fluorescence emission at 480 nm (red circles, left axis); and scaled-up ellipticity at 222 nm (green squares, right axis). (B) The same spectroscopic probes as above, monitored for ΔImpα3. Experiments were carried out at 4 μM of protein concentration (in both species and for all techniques) at 298 K and pH 7.8. (For interpretation of the references to color in this figure legend, the reader is referred to the web version of this article.)

The time-resolved anisotropy measurements of both species were fitted to two exponentials at any GdmCl concentration (Fig. 6A). Two distinct regions could be identified based on all these measurements: (a) the first region, from 0 to ~2 M GdmCl, where we observed a small decrease in the steady-state fluorescence anisotropy, $< r >_{ss}$, of the samples from ~0.19 to ~0.17; and (b) a second region from 2 to 5 M GdmCl, where the $< r >_{ss}$ of the protein substantially decreased from ~0.17 to ~0.09 (Table SM 2). Considering that control experiments revealed that the mean fluorescence lifetime, $< \tau >$, of the full-length protein concomitantly decreased from ~5 to ~3 ns upon increasing the denaturant concentration up to 5.5 M, these data strongly suggest that high denaturant concentrations were causing protein dissociation, which must be coupled to its unfolding. Indeed, the time-resolved anisotropy measurements of Impα3 confirm this conclusion: the $< r >_{ss}$ decays became much faster at high denaturant concentrations, despite the large increase in the solution viscosity (Fig. 6B). From 0 to ~2 M GdmCl the longer rotational correlation time of the protein, ϕ_2, remained essentially constant, and from 2 to 5 M GdmCl, it progressively decreased from ~35 to ~4 ns (Fig. 6C). To sum up, at low GdmCl concentrations, a structural rearrangement of quaternary structure of Impα3 was taking place, which was not accompanied by any oligomer dissociation, and at large concentrations of GdmCl, protein dissociation coupled to monomer unfolding occurred.

For ΔImpα3, we also observed a different behaviour to that found for Impα3 for each of the three steady-state probes (Fig. 5B), thus pinpointing that the unfolding was not a two-state process for this protein either. However, the behaviour for two of the spectroscopic probes was different to that observed for intact Impα3; only the ANS fluorescence showed a similar dumb-bell shape, as observed for Impα3, but with a maximum at ~0.75 M GdmCl (Fig. 5B, red circles), instead of at 1.5 M (Fig. 5A, red circles). This denaturant concentration at which ANS intensity reached a maximum is the same as that where the

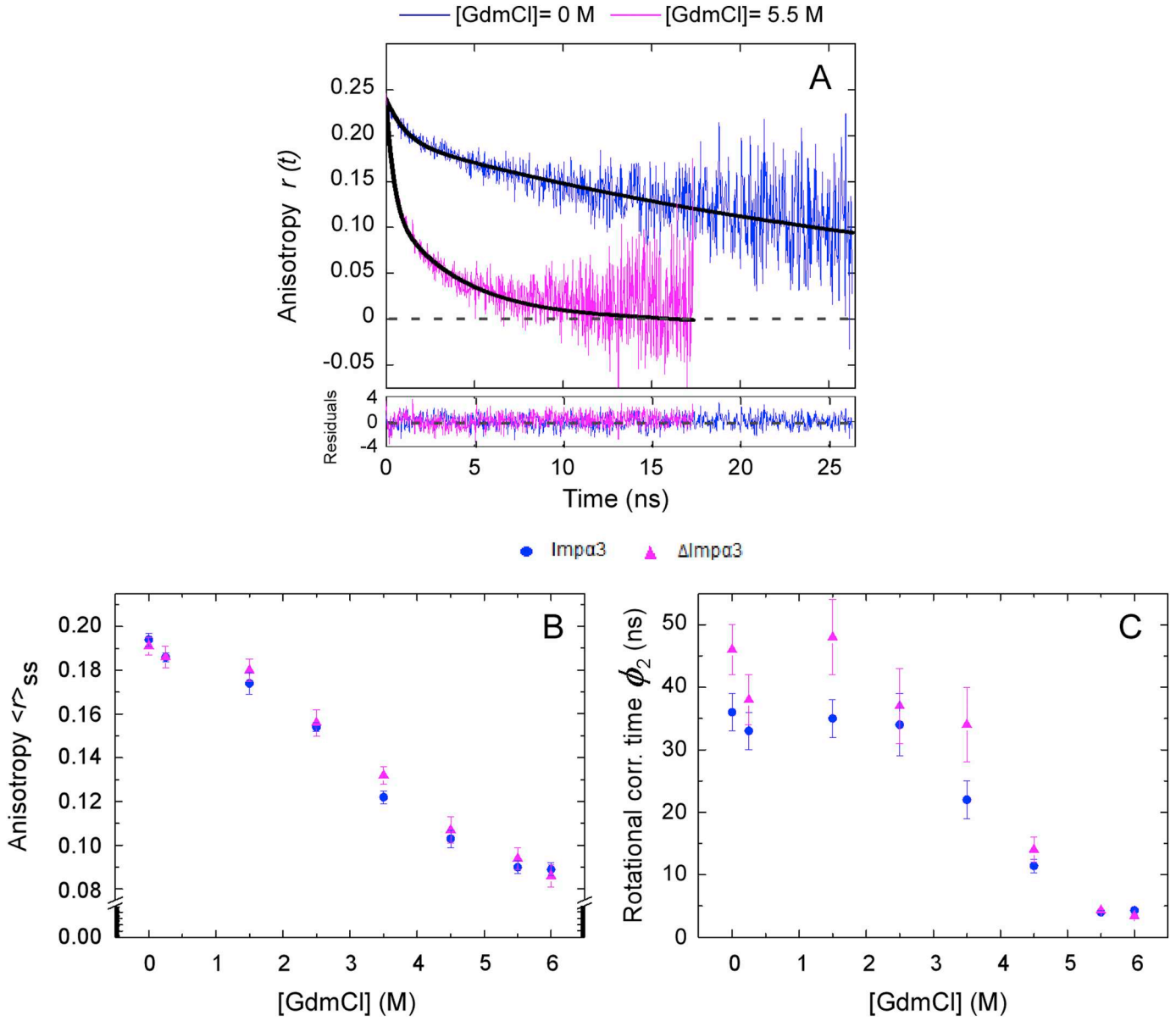

Fig. 6. Chemical denaturations followed by steady-state anisotropy, $< r >_{ss}$, and correlation time-dependent fluorescence. (A) Fluorescence anisotropy decays obtained at 7.5 μM for Impα3 in the absence of GdmCl (blue line) and in the presence of 5.5 M of the denaturant (pink line). The best fits of Eq. (4) to the experimental data are represented by a solid black curve. Changes in the $< r >_{ss}$ (B) and in the long rotational correlation time, ϕ_2, (C) as the concentration of GdmCl was increased. Experiments were carried out at 298 K (25 °C). (For interpretation of the references to color in this figure legend, the reader is referred to the web version of this article.)

behaviour of the intrinsic fluorescence and CD titration curves changed. The intrinsic fluorescence and far-UV CD titrations showed two regions: (i) between 0 and 0.75 M GdmCl, the ellipticity at 222 nm and the fluorescence intensity changed linearly, with an increase in the ellipticity value (in absolute value) at 222 nm (suggesting a larger population of helical structure as the concentration of denaturant increased or a different environment for the aromatic residues), concomitantly with an increase in the fluorescence; and (ii) between 0.75 M to 5 M, in the case of intrinsic fluorescence a flat sigmoidal-like titration (without unfolding baseline) was observed, whereas in CD a linear decrease of the ellipticity (in absolute value) was measured, similar to that in the intact protein (Fig. 5A, green squares). On the other hand, the overall changes detected in the steady-state and time-resolved fluorescence anisotropy of ΔImpα3 as a function of denaturant concentration were very similar to the ones previously described for Impα3 (Table SM 2). Briefly, the small decrease detected in the steady-state fluorescence anisotropy of ΔImpα3 at low concentrations of denaturant was not accompanied by any variation of its ϕ_2; again, as the concentration of GdmCl was increased above ~1.5–2 M, both the steady-state anisotropy and the ϕ_2 of the truncated protein decreased significantly indicating the occurrence of a coupled dissociation and unfolding of the truncated protein. The value of ϕ_2 (between 4 and 6 ns) observed in both proteins at 6 M GdmCl is typical of completely unfolded proteins [60], and reports on the isomeric rotation of the indole ring, since at these denaturant concentrations the overall rotational time of the molecule has not a measurable effect on the anisotropy.

4. Discussion

4.1. The native structure of the two importins was highly similar but their stabilities were different

The first conclusion of our studies is that the tertiary environment around the 6 tyrosines and 6 tryptophans in Impα3 was not affected by the removal of the IBB; however, the percentage of secondary structure was slightly modified (as measured by the changes in ellipticity at 222 nm), increasing in ΔImpα3 (~5%); alternatively, this increase in absolute value of the ellipticity could be explained as local conformational changes of aromatic residues, such as phenylalanines and histidines, which also absorb at 222 nm [61,62], occurring in ΔImpα3. That is, we can conclude that the presence of the IBB is not important to attain the tertiary structure of the whole protein, nor most of the secondary structure. However, its removal led to a more expanded conformation of the protein (Fig. 2B) and to a larger flexibility (see below), as shown by the smaller thermal-denaturation midpoint.

The acquisition of the secondary and tertiary structure, together with the burial of solvent-exposed hydrophobic regions, occurred concomitantly and in an identical manner (at both extremes of pH) in the two proteins (Fig. 1): only between pH 7.0 and 10.0, both proteins had a native-like structure. This indicates that the IBB domain does not have any influence on the overall electrostatic features of Impα3. The fact that the populated species at low pH in both proteins showed a large ANS binding suggests that they are probably molten globules [42], although we could not test by CD or fluorescence the lack of thermal unfolding due to sample precipitation.

The conformational stability of both species at physiological pH was very different, the one of Impα3 being the larger. This can be explained because although the IBB domain is a rather independent region [4], it makes hydrophobic, polar and van der Waals contacts with the NLS binding region of Impα3, thus stabilizing specific polypeptide patches, and then as a consequence having an overall stabilizing effect also on the whole protein structure. Similar differences between the apparent thermal denaturation midpoints (~10 K (10 °C)) of species derived from Importin α1 of *Xenopus laevis* have been reported [63]. This difference in stability between the truncated and the intact importins is also mirrored in the higher activation energy required in the two-state irreversible process (Fig. 5) for Impα3; in fact, it could be argued that the sole 64-residue-long IBB was responsible for the 100 kJ/mol increase of the activation energy in the thermal unfolding of Impα3.

Although we could not determine the thermodynamic conformational stability of both importins, the low value of the apparent thermal midpoint (332 K (59 °C)) suggests a high protein flexibility (which is larger in ΔImpα3). This flexibility has been proposed as one of the most important characteristics of Impα3 in recognizing rare topologies of the NLS polypeptides of their cargos [20,21]. Furthermore, a large flexibility has been suggested to be a general, important feature of other α-helix-repeat proteins [64,65].

4.2. Both importins were self-associating species

There are in the literature several importins described to form homodimers in solution and/or in the solved crystal structures when in isolation [17,66–68] or in the presence of their cargos [69]. The self-association constant for a dimer-monomer equilibrium in *Xenopus* importin α is ~20 μM [68], within the same range of that reported in this work for Impα3 (17 ± 6 μM, as determined by ITC, Fig. S1B). Therefore, it seems that there is a certain tendency for the members of the importin family to form oligomers; in fact, it has been suggested that this self-association could work as a mechanism of auto-inhibition [17]. Moreover, it has been shown that Impα3 is capable of heterodimerizing (with a high affinity) with importin α8, which shares a high structural similarity with Impα3 [70,71]; the self-association of Impα3, described in this work, could also function as a regulatory mechanism to control the heterodimer formation with importin α8, and in the end the binding of NLS cargos.

Although a dimer-monomer equilibrium could be fitted to the ITC data obtained for Impα3, we cannot rule out the presence of higher-order oligomers as suggested by the BN-PAGE (Fig. 2A), SAXS (Fig. SM 4A) and AU-SV (Fig. 2C). For ΔImpα3, the population of those higher-order oligomers was more abundant (as judged by visual inspection of the bands in the gel), and we could not determine any dissociation constant in the concentration range explored. Then, the tendency to form self-associated species is higher in ΔImpα3 than in Impα3; this is probably due to the fact that upon removal of IBB domain a large hydrophobic surface (the one where the NLS region of the cargo protein binds) is solvent-exposed, and could therefore act as a self-association surface. However, the fact that Impα3 self-associates indicates that not only the region exposed upon removal of the IBB is responsible for protein association, but rather there are other polypeptide patches along with the ten ARM units which must be involved in the oligomerization interface.

4.3. Both importins showed a complex unfolding pathway

The lack of identical curves (Fig. 5A and B) in the three steady-state spectroscopic probes used (namely, intrinsic fluorescence, ANS-fluorescence and far-UV CD) indicate that the unfolding of both proteins was not two-state [59]. Rather, in both cases, it must involve the presence of at least one intermediate.

The equilibrium unfolding of Impα3, which possesses 521 residues and ten ARM repeats, seems to unfold *via* an intermediate which occurred already at very small GdmCl concentrations (between 0 and 1.5 M); this intermediate was also a dimer (as judged by the small changes in $< r >_{ss}$ and ϕ_2 in that concentration range, Table SM 2), and it must undergo a quaternary rearrangement, which causes the exposure to the solvent of hydrophobic surfaces (as judged by the large increase of ANS fluorescence; Fig. 5A, red circles). This intermediate state, with non-native quaternary structure, had a lower fluorescence and a lower amount of secondary structure (approximately a 20% less; Fig. 5A, green squares) than the native state. We do not know at the moment whether this intermediate state was similar to that detected in the thermal denaturation experiments; in fact, it has been suggested

that the thermal and chemical denatured states of proteins could be different [72]. Above 1.5 M concentration of GdmCl, dissociation and monomer unfolding occurred concomitantly as concluded from: (i) the three steady-state methodologies; and (ii) the lifetime and time-resolved anisotropy measurements (Table SM 2). This unfolding and dissociation occurred in a non-cooperative fashion, especially from the point of view of the melting of the secondary structure (far-UV CD). It means that the folding landscape of the protein was very broad, as shown in our MD simulations, and as it has been described by using MD and atomic force microscopy (AFM) in other α-helical-repeat proteins with a large number of repeat units [73].

On the other hand, the folding intermediate in ΔImpα3 seemed to form at a lower GdmCl concentration (0.75 M) than in Impα3, (1.5 M), probably due to the smaller stability of the truncated species (see above). This intermediate has not a native-like tertiary or quaternary structure and its exposure to the solvent of hydrophobic patches was, as well, not native-like (as judged from ANS fluorescence, Fig. 5B, red circles), although both $< r >_{ss}$ and ϕ_2 did not change substantially in the 0 to 0.75 M GdmCl range (Table SM 2). However, its spectroscopic features were different from those observed for the intermediate species in Impα3. First, the intermediate state in ΔImpα3 had a larger fluorescence than the native one (hyperfluorescent intermediate states have been observed in the unfolding of other α-helix-repeat proteins, [74] and references therein); and second, its helicity, as judged from the CD titration curves (Fig. 4B, green squares), was larger than that of the native state (that is, we could consider that the intermediate showed an hyper-ellipticity). Then, the intermediate state was more helical, or alternatively the orientation for some of the aromatic residues (which also absorb at 222 nm [61,62]) changed as the GdmCl concentration was increased; in addition, this intermediate contained a large amount of solvent-exposed hydrophobic patches. Above a concentration of 0.75 M GdmCl, the dissociation and unfolding of the monomers in ΔImpα3 occurred, as well, in a non-cooperative way. Therefore, the similarities between the different spectroscopic curves of both importins at high GdmCl concentrations allow us to conclude that these sections of the curves were monitoring the dissociation and unfolding of the monomers, but what we do not know is whether the unfolding of the ten ARM units occurred in a single step, or there was a fraying in the unfolding of consecutive repeats from one terminus of the protein to the other. Reports on the unfolding processes of other α-helical-repeat proteins have suggested that the cooperativity of the denaturation breaks down when the protein contains more than six or seven repeats of ankyrin motifs (which is smaller than the ARM one) [74], and then the unfolding process is not two-state any longer, as the protein has a quite broad landscape with partially folded states very close in energy [75,76]. It is tempting to suggest that for importin α, which has ten ARM repeats, the unfolding was not cooperative, as indicated by our MD unfolding simulations, and that some units unfold before others (in that shift progressing through the different ARM units, observed in our MD simulations). The removal of the IBB partially altered this scenario, since another intermediate with different structural features was populated but non-cooperativity was still present.

5. Conclusions

We described that human Impα3 is a dimeric protein with a low stability, which acquired a native structure in a narrow pH range (between 7.0 and 10.0). The high instability results in a large flexibility, that is likely responsible for the ability of Impα3 to recognize NLS regions of different origins. The removal of its N-terminal IBB domain destabilizes the protein to a large extent (and therefore increases its flexibility), but it keeps its ability to self-associate.

Authors contribution

CD-G, FH, AMG, ACA, BR, JG, MP, AC and JLN designed the experiments and the research methodology. CD-G, FH, AMG, JRL-O, AA, CA, ACA, BR and JLN carried out the experiments. CD-G, FH, AMG, ACA, MP, JRL-O, AA, CA, AC, JG, BR and JLN analyzed the data. JKF and JLI provided materials and analyzed the results. All authors wrote, revised and corrected the manuscript.

Acknowledgements and funding

We thank both reviewers for suggestions and discussion. This work was supported by Spanish Ministry of Economy and Competitiveness and European FEDER Funds (MCIU/AEI/FEDER, EU) [RTI2018-097991-B-I00 to JLN and JG, BFU2016-75471-C2-1-P to CA, PGC2018-094548-B-I00 to AA and BIO2016-78020-R to ACA], Basque Country [IT-1175-19 to AA], GVA and EU-FEDER funds “Una forma de hacer Europa” [GVA-IDIFEDER 2018/020] and Portuguese FCT [UIDB/04565/2020 and SAICTPAC/0019/2015 to AC and MP]. AUC SV assays were performed at the Molecular Interactions Facility at the CIB Margarita Salas. CD-G acknowledges Medical Biochemistry and Biophysics Doctoral Programme (M2B-PhD) FCT reference: SFRH/PD/BD/135154/2017. BR acknowledges the kind hospitality and use of computational resources in the European Magnetic Resonance Center (CERM), Sesto Fiorentino (Florence), Italy.

Declaration of competing interest

The authors declare no competing interests.

Appendix A. Supplementary data

Supplementary data to this article can be found online at https://doi.org/10.1016/j.bbagen.2020.129609. There are two tables and five figures in the Supplementary Material: fluorescence spectra of both importin species and their thermal denaturations at pH 7.8 (Fig. SM1); CD spectra of both importin species and their thermal denaturations at pH 7.8 (Fig. SM2); the WB results (Fig. SM3); the SAXS and the ITC titrations for both proteins (Fig. SM4); and chemical-denaturation reversibility of both proteins explored by fluorescence and far-UV CD (Fig. SM5).

References

[1] M. Stewart, Molecular mechanism of the nuclear protein import cycle, Nat. Rev. Mol. Cell Biol. 8 (2007) 195–208.
[2] J. Bednenko, G. Cingolari, L. Gerace, Nucleo-cytoplasmic transport navigating the channel, Traffic 4 (2003) 127–135.
[3] G. Cingolani, J. Bednenko, M.T. Gillespie, L. Gerace, Molecular basis for the recognition of a non classical nuclear localization signal by importin beta, Mol. Cell 10 (2002) 1345–1353.
[4] D.S. Goldfarb, A.H. Corbett, D.A. Mason, M.T. Harreman, S.A. Adam, Importin α: a multipurpose nuclear-transport receptor, Trends Cell Biol. 14 (2004) 505–514.
[5] S. Milles, D. Mercadante, I.V. Aramburu, M.R. Jensen, N. Banterle, C. Koeheler, S. Tyagi, J. Clarke, S.L. Shammas, M. Balckledge, F. Gräter, E.A. Lemke, Plasticity of an ultrafast interaction between nucleoporins and nuclear transport receptors, Cell 163 (2015) 734–745.
[6] E. Izaurralde, U. Kutay, C. von Kobbe, I.W. Mattaj, D. Görlich, The asymmetric distribution of the constituents of the Ran system is essential for transport into and out of the nucleus, EMBO J. 16 (1997) 6535–6547.
[7] Y. Miyamoto, K.L. Loveland, Y. Yoneda, Nuclear importin α and its physiological importance, Commun. Integr. Biol. 5 (2012) 220–222.
[8] Y. Yasuda, Y. Miyamoto, T. Yamashiro, M. Asally, A. Masui, C. Wong, K.L. Loveland, Y. Yoneda, Nuclear retention of importin α coordinates cell fate through changes in gene expression, EMBO J. 31 (2012) 83–94.
[9] T. Cagatay, Y.M. Chook, Karyopherins in cancer, Curr. Opin. Cell Biol. 52 (2018) 30–42.
[10] R.A. Pumroy, G. Cingolani, Diversification of importin-alpha isoforms in cellular trafficking and disease states, Biochem. J. 466 (2015) 13–28.
[11] D.A. Mason, D.E. Stage, D.S. Goldfarb, Evolution of the metazoan-specific importin alpha gene family, J. Mol. Evol. 68 (2009) 351–365.
[12] A. Mahipal, M. Malafa, Importins and exportins as therapeutic targets in cancer, Pharmacol Ther. 164 (2016) 135–143.
[13] K.M. Smith, S. Tsimbalyuk, M.G. Edwards, E.M. Cross, J. Batra, T.P. Soares da Costa, D. Aragao, C.F. Basler, J.K. Forwood, Structural basis for importin alpha 3 specificity of W proteins in Hendra and Nipah viruses, Nat. Commun. 9 (2018) 3703.

[14] G. Cingolani, C. Petosa, K. Weis, C.W. Muller, Structure of importin-β bound to the IBB domain of importin-α, Nature 399 (1999) 221–229.
[15] S.J. Lee, Y. Matsuura, S.M. Lisu, M. Stewart, Structural basis for nuclear import complex dissociation by RanGTP, Nature 435 (2005) 693–696.
[16] B. Kobe, Autoinhibition by an internal nuclear localization signal revealed by the crystal structure of mammalian importin α, Nat. Struct. Biol. 6 (1999) 388–397.
[17] H. Miyatake, A. Sanjoh, S. Unzai, G. Mtsuda, Y. Tatsumi, Y. Miyamoto, N. Dohmae, Y. Aida, Crystal structure of human importin α1 (Rch1) revealing a potential autoinhibition mode involving homodimerization, PLoS One 20 (2015) e0115995.
[18] A. Cook, F. Bono, M. Jinek, E. Conti, Structural biology of the nucleo-cytoplasmic transport, Annu. Rev. Biochem. 76 (2007) 647–671.
[19] R.S. Sankhala, R.K. Lokareddy, S. Begum, R.A. Pumroy, R.E. Gilian, G. Cingolani, Three-dimensional context rather than NLS amino acid sequence determines importin α subtype specificity for RCC1, Nat. Commun. 8 (2017) 979.
[20] R.A. Pumroy, S. Ke, D.J. Hart, U. Zacharie, G. Cingolani, Molecular determinants for nuclear import if influenza A PB2 by importin alpha isoforms 3 and 7, Structure 23 (2015) 374–384.
[21] S.C. Gill, P.H. von Hippel, Calculation of protein extinction coefficients from amino acid sequence data, Anal. Biochem. 182 (1989) 319–326.
[22] J.L. Neira, M. Román-Trufero, L.M. Contreras, J. Prieto, G. Singh, F.N. Barrera, M.L. Renart, M. Vidal, The transcriptional repressor RYBP is a natively unfolded protein which folds upon binding to DNA, Biochemistry 48 (2009) 1348–1360.
[23] J.L. Neira, F. Hornos, J. Bacarizo, A. Cámara-Artigas, J. Gómez, The monomeric species of the regulatory domain of tyrosine hydroxylase has a low conformational stability, Biochemistry 55 (2017) 3418–3431.
[24] Y. Nozaki, The preparation of guanidine hydrochloride, in: C.H.W. Hirs, S.N. Timasheff (Eds.), Methods in Enzymology, Vol. 26 Academic, New York, 1972, pp. 43–50.
[25] J.A. Poveda, M. Prieto, J.A. Encinar, J.M. González-Ros, C.R. Mateo, Intrinsic tyrosine fluorescence as a tool to study the interaction of the shaker B "ball" peptide with anionic membranes, Biochemistry 42 (2003) 7124–7132.
[26] R.F. de Almeida, L.M. Loura, M. Prieto, A. Watts, A. Fedorov, F.J. Barrantes, Structure and dynamics of the gammaM4 transmembrane domain of the acetylcholine receptor in lipid bilayers: insights into receptor assembly and function, Mol. Membr. Biol. 23 (2006) 305–315.
[27] J.R. Lakowicz, Principles of Fluorescence Spectroscopy, 2nd ed., Springer, New York, 1999.
[28] S. Benjwal, S. Verma, K.H. Röhm, O. Gursky, Monitoring protein aggregation during thermal unfolding in circular dichroism experiments, Protein Sci. 15 (2006) 635–639.
[29] A.M. Giudici, M.L. Molina, J.L. Ayala, E. Montoya, M.L. Renart, A.M. Fernandez, J.A. Encinar, A.V. Ferrer-Montiel, J.A. Poveda, J.M. Gonzalez-Ros, Detergent-labile, supramolecular assemblies of KcsA: relative abundance and interactions involved, Biochim. Biophys. Acta 1828 (2013) 193–200.
[30] J. Stetefeld, S.A. Mckenna, T.R. Patel, Dynamic light scattering: a practical guide and applications in biomedical sciences, Biophys. Rev. 8 (2016) 409–427.
[31] H. Schagger, G. von Jagow, Blue native electrophoresis for isolation of membrane protein complexes in enzymatically active form, Anal. Biochem. 199 (1991) 223–231.
[32] P. Schuck, Size-distribution analysis of macromolecules by sedimentation velocity ultracentrifugation and Lamm equation modeling, Biophys. J. 78 (2000) 1606–1609.
[33] T.M. Laue, B.D. Shah, T.M. Ridgeway, S.L. Pelletier, Interpretation of analytical sedimentation data for proteins, in: S.E. Harding, A.J. Rowe, J.C. Horton (Eds.), Analytical Ultracentrifugation in Biochemistry and Polymer Science, Royal Society of Chemistry, Cambridge, UK, 1992, pp. 90–125.
[34] B. Hammouda, Small angle scattering from branched polymers, Macromol. Theory Simul. 21 (2012) 372–381.
[35] M.J. Abraham, T. Murtola, R. Schulz, S. Páll, J.C. Smith, B. Hess, J. Lindahl, GROMACS: high performance molecular simulations through multi-level parallelism from laptops to supercomputers, SoftwareX 1–2 (2015) 19–25.
[36] A. Guglielmelli, B. Rizzuti, R. Guzzi, Stereoselective and domain-specific effects of ibuprofen on the thermal stability of human serum albumin, Eur. J. Pharm. Sci. 112 (2018) 122–131.
[37] L.M. Contreras, P. Sevilla, A. Cámara-Artigas, J.G. Hernández-Cifre, B. Rizzuti, F.J. Florencio, M.I. Muro-Pastor, J.G. de la Torre, J.L. Neira, The cyanobacterial ribosomal-associated protein LrtA from *Synechocystis sp.* PCC 6803 is an oligomeric protein in solution with chameleonic sequence properties, Int. J. Mol. Sci. 19 (2018) 1857-1-21.
[38] K. Lindorff-Larsen, S. Piana, K. Palmo, P. Maragakis, J.L. Klepeis, R.O. Dror, D.E. Shaw, Improved side-chain torsion potentials for the Amber ff99SB protein force field, Proteins 78 (2010) 1950–1958.
[39] W.L. Jorgensen, J. Chandrasekhar, J.D. Madura, R.W. Impey, M.L. Klein, Comparison of simple potential functions for simulating liquid water, J. Chem. Phys. 79 (1983) 926–935.
[40] S. Evoli, R. Guzzi, B. Rizzuti, Molecular simulations of β-lactoglobulin complexed with fatty acids reveal the structural basis of ligand affinity to internal and possible external binding sites, Proteins 82 (2014) 2609–2619.
[41] J.L. Neira, B. Rizzuti, J.L. Iovanna, Determinants of the pK_a values of ionizable residues in an intrinsically disordered protein, Arch. Biochem. Biophys. 598 (2016) 18–27.
[42] O.B. Ptitsyn, Molten globule and protein folding, Adv. Protein Chem. 47 (1995) 83–229.
[43] S. Pedersen, L. Nesgaard, R.P. Baptista, E.P. Melo, S.R. Kristensen, D.E. Otzen, pH-dependent aggregation of cutinase is efficiently suppressed by 1,8-ANS, Biopolymers 83 (2006) 619–629.
[44] H. Schagger, W.A. Cramer, G. von Jagow, Analysis of molecular masses and oligomeric states of protein complexes by blue native electrophoresis and isolation of membrane protein complexes by two-dimensional native electrophoresis, Anal. Biochem. 1994 (217) (1994) 220–230.
[45] E.H. Heuberger, L.M. Veenhoff, R.H. Duurkens, R.H. Friesen, B. Poolman, Oligomeric state of membrane transport proteins analysed with blue native electrophoresis and analytical ultracentrifugation, J. Mol. Biol. 317 (2002) 591–600.
[46] A. Nicke, J. Rettinger, E. Mutschler, G. Schmalzing, Blue native PAGE as a useful method for the analysis of the assembly of distinct combinations of nicotinic acetylcholine receptor subunits, J. Recept. Signal Transduct. Res. 19 (1999) 493–507.
[47] K.R. Vinothkumar, S. Raunser, H. Jung, W. Kühlbrandt, Oligomeric structure of the carnitine transporter CaiT from Escherichia coli, J. Biol. Chem. 281 (2006) 4795–4801.
[48] M. Mitrea, B. Chandra, M.C. Ferrolino, E.B. Gibbs, M. Tolbert, M.R. White, R.W. Kriwacki, Methods for physical characterization of phase-separated bodies and membrane-less organelles, J. Mol. Biol. 430 (2018) 4773–4805.
[49] J. Gómez, V.J. Hilser, D. Xie, E. Freire, The heat capacity of proteins, Proteins 22 (1995) 404–412.
[50] J. Gómez, E. Freire, Thermodynamic mapping of the inhibitor site of the aspartic protease endothiapepsin, J. Mol. Biol. 252 (1995) 337–350.
[51] J.M. Sánchez-Ruiz, J.L. López-Lacomba, M. Cortijo, P.L. Mateo, Differential scanning calorimetry of the irreversible thermal denaturation of thermolysin, Biochemistry 27 (1988) 1648–1652.
[52] F. Conejero-Lara, P.L. Mateo, F.X. Aviles, J.M. Sánchez-Ruiz, Effect of Zn^{2+} on the thermal denaturation of carboxypeptidase B, Biochemistry 30 (1991) 2067–2072.
[53] M.L. Galisteo, P.L. Mateo, J.M. Sánchez-Ruiz, Kinetic study on the irreversible thermal denaturation of yeast phosphoglycerate kinase, Biochemistry 30 (1991) 2061–2066.
[54] M.E. McCully, D.A.C. Beck, V. Daggett, Microscopic reversibility of protein folding in molecular dynamics simulations of the engrailed homeodomain, Biochemistry 47 (2008) 7079–7089.
[55] B. Rizzuti, V. Daggett, Using simulations to provide the framework for experimental protein folding studies, Arch. Biochem. Biophys. 531 (2013) 128–135.
[56] B. Rizzuti, V. Daggett, R. Guzzi, L. Sportelli, The early steps in the unfolding of azurin, Biochemistry 43 (2004) 15604–15609.
[57] M.L. López-Redondo, A. Contreras, A. Marina, J.L. Neira, The regulatory factor SipA is a highly stable beta-II class protein with a SH3 fold, FEBS Lett. 584 (2010) 989–994.
[58] U. Zachariae, H. Grubmüller, Importin-β: structural and dynamic determinants of a molecular spring, Structure 16 (2008) 906–915.
[59] S.E. Jackson, How do small single-domain proteins fold? Fold. Des. 3 (1998) R81–R91.
[60] O. Tcherkasskaya, J.R. Knutson, S.A. Bowley, M.K. Frank, A.M. Gronenbrog, Nanosecond dynamics of the single tryptophan reveals multi-state equilibrium unfolding of protein GB1, Biochemistry 39 (2000) 11216–11226.
[61] R.W. Woody, Circular dichroism, Methods Enzymol. 246 (1995) 34–71.
[62] S.M. Kelly, N.C. Price, The use of circular dichroism in the investigation of protein structure and function, Curr. Protein Pept. Sci. 1 (2000) 349–384.
[63] J. Falces, I. Arrgi, P.V. Knoarev, M.A. Urbaneja, D.I. Svergun, S.G. Taneva, S. Bañuelos, Recognition of nucleoplasmin by its nuclear transport receptor importin α/β: insights into a complete import complex, Biochemistry 49 (2010) 9756–9769.
[64] S.H. Yoshimura, T. Hirano, HEAT repeats – versatile arrays of amphiphilic helices working in crowded environments? J. Cell Sci. 129 (2016) 3963–3970.
[65] K. Manalatas-Cantos, M. Kschoonsak, C.H. Maering, D.I. Svergun, Solution structure and flexibility of the condensing HEAT-repeat subunit YCg1, J. Biol. Chem. 294 (2019) 13822–13829.
[66] E. Conti, M. Uy, L. Leighton, G. Blobel, J. Juriyan, Crystallographic analysis of the recognition of a nuclear localization signal by the nuclear import factor karyopherin alpha, Cell 94 (1998) 193–204.
[67] D. Görlich, S. Prehn, R.A. Laskey, E. Hartman, Isolation of a protein that is essential for the first step of nuclear protein import, Cell 79 (1994) 767–787.
[68] P. Percipalle, P.J. Butler, J.T. Finch, D.A. Jans, D. Rhodes, Nuclear localization signal recognition causes release of importin α from aggregates in the cytosol, J. Mol. Biol. 292 (1999) 263–273.
[69] H. Miyatake, A. Sanjoh, T. Murakami, H. Murakami, G. Matsuda, K. Hagiware, M. Yokoyama, H. Sato, Y. Miyamoto, N. Dohmae, Y. Aida, Molecular mechanism of HIV-1 Vpr for binding to importin α, J. Mol. Biol. 428 (2016) 2744–2757.
[70] C. Kimoto, T. Moriyama, A. Tusjii, Y. Igarashi, C. Obuse, Y. Miyamoto, M. Oka, Y. Yoneda, Functional characterization of importin α8 as a classical nuclear localization signal receptor, Biochim. Biophys. Acta, Mol. Cell Res. 1853 (2015) 2676–2683.
[71] Y. Miyamoto, M. Oka, Data on dimer formation between importin α subtypes, Data in Brief 7 (2016) 1248–1253.
[72] A. Narayan, K. Bhattacharjee, A.N. Naganathan, Thermally versus chemically denatured protein states, Biochemistry 58 (2019) 2519–2523.
[73] D. Serquera, W. Lee, G. Settanni, P.E. Marszalek, E. Paci, L.S. Itzhaki, Mechanical unfolding of an ankyrin repeat protein, Biophys. J. 98 (2010) 1294–1301.
[74] N.D. Werbeck, L.S. Itzhaki, Probing a moving target with a plastic unfolding intermediate of an ankyrin-repeat protein, Proc. Natl. Acad. Sci. U. S. A. 104 (2007) 7863–7868.
[75] D. Barrick, D.U. Ferreiro, E.A. Komives, Folding landscapes of ankyrin repeat proteins: experiments meet theory, Curr. Opin. Struct. Biol. 18 (2008) 27–34.
[76] D.U. Ferreiro, E.A. Komives, The plastic landscape of repeat proteins, Proc. Natl. Acad. Sci. U. S. A. 104 (2007) 7735–7736.